1-1-2017

Mechanistic Insights into the Radical S-Adenosyl L-Methionine Enzyme MFTC

Bulat Khaliullin
University of Denver

Mechanistic Insights into the Radical S-Adenosyl L-Methionine Enzyme MFTC

Abstract

Mycofactocin is a putative peptide-derived redox cofactor in *Mycobacterium* family. Its putative biosynthetic pathway is encoded by the operon *mftABCDEF*. The initial step of this pathway is a posttranslational modification of a peptide precursor MftA, which is catalyzed by MftC enzyme. This modification only occurs in the presence of chaperone MftB. Here, we demonstrate that MftC is a radical S-adenosyl L-methionine (SAM) enzyme and we examine its catalytic mechanism. We show that the modification of MftA requires two equivalents of SAM and is implemented in two steps: (i) the decarboxylation of a C-terminal tyrosine, resulting in formation of an intermediate with a carbon-carbon double bond, and (ii) the cross-linking of the tyrosine with the penultimate valine, leading to formation of a cyclized product. We also show that MftC is able to modify unnatural peptide substrates, resulting in formation of specific and non-specific products.

Document Type

Thesis

Degree Name

M.S.

Department

Chemistry and Biochemistry

First Advisor

John A. Latham, Ph.D.

Second Advisor

Schuyler van Engelenburg

Third Advisor

Martin Margittai

Keywords

Mechanism, Mycofactocin pathway, Peptide modification, Radical SAM enzyme, Radical S-adenosyl L-methionine enxyme, SPASM domain

Subject Categories

Biochemistry, Biophysics, and Structural Biology | Chemistry

MECHANISTIC INSIGHTS INTO THE RADICAL S-ADENOSYL L-METHIONINE ENZYME MFTC

_____

A Thesis

Presented to

the Faculty of Natural Sciences and Mathematics

University of Denver

_____

In Partial Fulfillment

of the Requirements for the Degree

Master of Science

_____

by

Bulat Khaliullin

June 2017

Advisor: John A. Latham

Author: Bulat Khaliullin
Title: MECHANISTIC INSIGHTS INTO THE RADICAL S-ADENOSYL L-METHIONINE ENZYME MFTC
Advisor: John A. Latham
Degree Date: June 2017

Abstract

Mycofactocin is a putative peptide-derived redox cofactor in *Mycobacterium* family. Its putative biosynthetic pathway is encoded by the operon *mftABCDEF*. The initial step of this pathway is a posttranslational modification of a peptide precursor MftA, which is catalyzed by MftC enzyme. This modification only occurs in the presence of chaperone MftB. Here, we demonstrate that MftC is a radical S-adenosyl L-methionine (SAM) enzyme and we examine its catalytic mechanism. We show that the modification of MftA requires two equivalents of SAM and is implemented in two steps: (i) the decarboxylation of a C-terminal tyrosine, resulting in formation of an intermediate with a carbon-carbon double bond, and (ii) the cross-linking of the tyrosine with the penultimate valine, leading to formation of a cyclized product. We also show that MftC is able to modify unnatural peptide substrates, resulting in formation of specific and non-specific products.

List of Publications

Khaliullin, B.; Aggarwal, P.; Bubas, M.; Eaton, G. R.; Eaton, S. S.; Latham, J. A. Mycofactocin biosynthesis: modification of the peptide MftA by the radical S-adenosylmethionine protein MftC. *FEBS Letters* **2016**, *590*, 2538-2548.

Khaliullin, B.; Ayikpoe, R.; Tuttle, M.; Latham, J. A. Mechanistic details of the mycofactocin biosynthetic protein MftC, a radical-S-adenosylmethionine protein. Under review at *J. Biol. Chem.*, MS ID: JBC/2017/795682.

Table of Contents

List of Figures

CHAPTER ONE: INTRODUCTION

Peptide-derived redox quinocofactors and their biosynthetic pathways

Redox cofactors are a class of low-molecular weight compounds that serve as electron carriers in cell metabolism. Based on the composition, they can be divided into two groups: organic and inorganic cofactors. Within the organic category, quinone cofactors are the most notable. Some of these quinocofactors are formed via specific biosynthetic pathways that catalyze consecutive post-translational modifications of ribosomally synthesized peptide precursors that occur on side chains of tryptophan [1] or tyrosine [2]. Currently, five peptide-derived quinocofactors have been identified: PQQ, TTQ, CTQ, TPQ, and LTQ [3] (Figure 1). Except for PQQ, these cofactors are synthesized *in situ* of their respective enzymes. The biochemical role of the quinocofactors is to serve as assistants of enzymes which oxidize alcohols [4] or primary amines [5] into corresponding aldehydes.

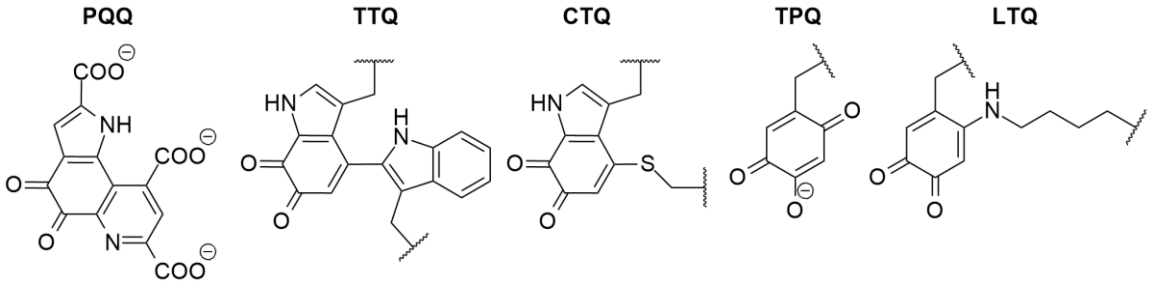

Figure 1. Structures of the identified peptide-derived quinocofactors.

PQQ Biosynthesis

PQQ, or pyrroloquinoline quinone, was discovered as a prosthetic group of glucose dehydrogenase in *Bacterium anitratum*, in 1964 [6]. In general, PQQ serves as a prokaryotic cofactor in more than 125 bacterial species [7]. In bacteria, PQQ mainly functions as a catalytic cofactor of alcohol and glucose dehydrogenases operating in the periplasm of Gram-negative bacteria [8]. The reduced form of PQQ, $PQQH_2$, is formed during catalysis of these enzymes. $PQQH_2$ is then oxidized back to PQQ by a cytochrome in two sequential steps [4]. The formation of reduced cytochrome indirectly triggers ATP synthesis, and therefore, energy storage by cell [4].

The biosynthetic pathway of PQQ consists of the gene products encoded by the *pqqABCDEF* operon (Figure 2) [7]. PqqA is a peptide of 20-30 amino acids length, containing conserved residues of glutamate and tyrosine which are the main constituents of PQQ. The initial step of the PQQ synthesis is the formation of a carbon-carbon bond between side chains of these residues, which is achieved by radical reaction performed by PqqE enzyme [9]. PqqE is a radical S-adenosyl L-methionine (SAM) protein that catalyzes the reductive cleavage of SAM (discussed below), which initiates a free-radical reaction resulting in the carbon-carbon bond formation between glutamate and tyrosine [10]. This reaction requires PqqD, a small (90 amino acids) protein that serves as a peptide chaperone delivering the peptide PqqA to PqqE [11]. It has been proposed that the cross-linked PqqA product is cleaved at the glutamate and the tyrosine into a low-molecular intermediate by the pathway protease PqqF [12]. In this intermediate, the amino-group of the glutamate undergoes spontaneous condensation with hydroxyl group of the tyrosine [3, 12]. The resulting species is then oxidized by an unknown enzyme to

3a-(2-amino-2-carboxyethyl)-4,5-dioxo-4,5,6,7,8,9-hexahydroquinoline-7,9-dicarboxylic acid (AHQQ) which is the substrate of PqqC enzyme [3]. PqqC catalyzes the final step of the pathway, which is a multi-step eight-electron oxidation and ring cyclization of AHQQ to produce PQQ, with help of O_2 as an electron acceptor [13]. It has been suggested that produced PQQ is transferred by PqqB to the periplasm [14]. PqqB is also speculated to oxidize the tyrosine residue in PqqA prior to the cross-linking with the glutamate [7, 12].

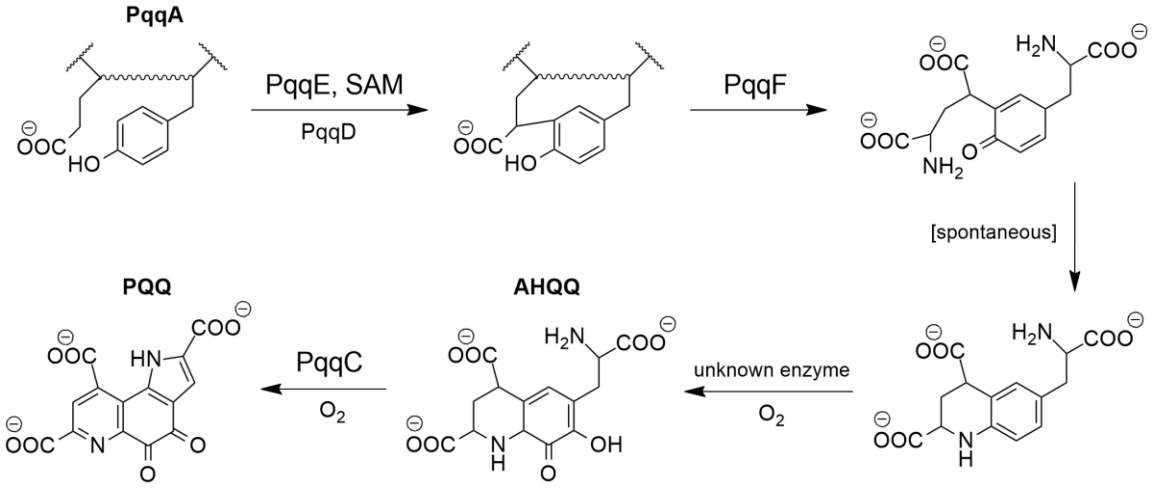

Figure 2. Biosynthetic pathway of PQQ.

TTQ Biosynthesis

TTQ, or tryptophan tryptophylquinol, was first identified and confirmed as a prosthetic group of methylamine dehydrogenase (MADH) in *Methylobacterium extorquens* AM1, in 1991 [15]. This cofactor is utilized by MADH and aromatic amine dehydrogenase (AADH) that are located in periplasmic space in bacteria. In the process of the catalysis, TTQ is reduced to $TTQH_2$, which is then reoxidized by the single-electron transfer copper proteins (cupredoxins) through formation of an *o*-semiaminoquinone intermediate [16].

TTQ is synthesized from two tryptophan residues which are posttranslationally modified within the polypeptide chain of the enzymes (Figure 3). The first step of its biosynthesis is hydroxylation of one of the tryptophan residues at C7 [17]; this process is speculated to be autocatalytic [18]. The resulting product (pre-MADH) is a substrate for an enzyme MauG, which completes the biosynthesis of TTQ [17]. MauG shares 30% sequence similarity with cytochrome c peroxidases and contains two c-type hemes as well; nevertheless, it does not act like a typical peroxidase [19]. The entire reaction performed by MauG proceeds in three successive two-electron oxidation steps: (i) the diradical cross-linking of indole rings of the Trp residues [20]; (ii) the addition of the second hydroxyl group at C6 in the hydroxylated Trp residue; (iii) the oxidation of the produced *o*-quinol into *o*-quinone [21]. The oxidants used in the reaction are O_2 (plus electron donor) or H_2O_2, which are carried by the heme groups of MauG, executing the whole catalysis [21].

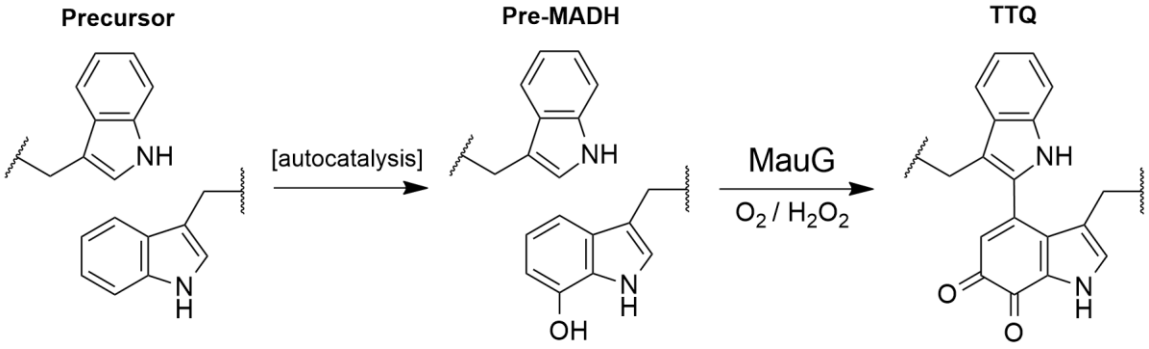

Figure 3. Biosynthetic pathway of TTQ in MADH.

CTQ Biosynthesis

CTQ, or cysteine tryptophyl quinone, was found in a crystal structure of quinohemoprotein amine dehydrogenase (QHNDH) in *Paracoccus denitrificans*, in 2001 [22]. Later, this cofactor was also detected in two amino acid oxidases, LodA (L-lysine oxidase) [23] and GoxA (glycine oxidase) [24], in *Marinomonas mediterranea*. During the catalysis implemented by all these enzymes, CTQ is reduced to $CTQH_2$ which is reoxidized by cytochrome c550 [25] or a blue copper protein azurin [26] which provide electron transport for the membrane-associated respiratory chain [25].

Although CTQ biosynthesis is similar to the TTQ biosynthesis (Figure 4), it is currently not fully understood. In case of LodA and GoxA oxidases, the first step is an autocatalytic hydroxylation of an indole ring of a tryptophan residue at C7 position. It has recently been shown that copper in high oxidation state is required for this process, and several variants of the mechanism have been proposed [18]. The next step includes cross-linking between Cys residue and the hydroxylated Trp residue, as well as the insertion of the second oxygen group into indole ring of the tryptophan at C6 position. This reaction is catalyzed by FAD-dependent monooxidases LodB and GoxB that are co-expressed with LodA and GoxB, respectively. In case of QHNDH, the enzyme involved in CTQ formation has been proposed to be QhpG [27]. This protein is encoded in the complementary strand with respect to the *qhp* operon and it shares sequence homology to FAD-dependent monooxygenases. It is speculated that QhpG may catalyze the initial hydroxylation of the tryptophan, whereas the subsequent step may be executed in a MauG-like fashion, by means of two c-type hemes located in the α-subunit of QHNDH.

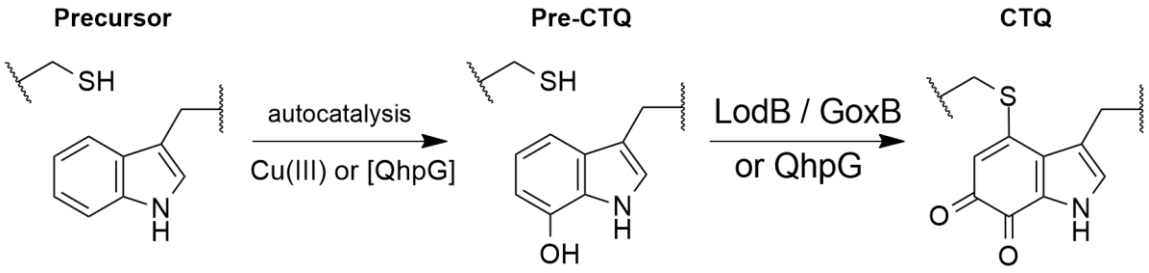

Figure 4. Biosynthetic pathway of CTQ in LodA/GoxA and QHNDH.

TPQ Biosynthesis

TPQ, or trihydroxyphenylalanine quinone (topaquinone), was discovered in bovine serum copper amine oxidase (CAO), in 1990 [28]. This cofactor is found in copper amine oxidases in both prokaryotic and eukaryotic organisms [3, 5]. The biosynthesis of TPQ is simple (Figure 5), since it does not involve cross-linking with other amino acid residues. The precursor is a tyrosine residue in the conserved Asn-Tyr-Asp/Glu motif surrounded by hydrophobic amino acids, in the polypeptide chain of CAO [29]. Topaquinone is synthesized by hydroxylation of a phenol ring of the tyrosine residue at C2- and C5-positions followed by its oxidation into an *o*-quinone. The entire process is fully autocatalytic and requires only a copper(II) ion and molecular oxygen, proceeding through formation of ligand-to-metal charge transfer complexes [30].

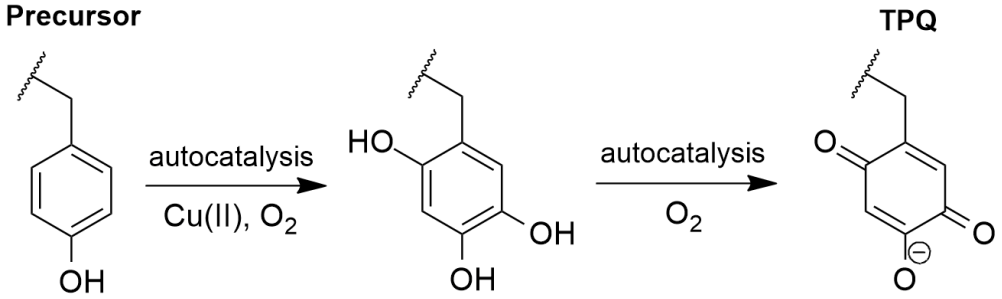

Figure 5. Biosynthesis of TPQ in CAO.

LTQ Biosynthesis

LTQ, or lysyl tyrosine quinone, was identified in lysyl oxidase from bovine aorta, in 1996 [31]. This enzyme is the only protein where LTQ has been found. The function of this enzyme is to oxidize lysine residues in collagen and elastin fibrous proteins, which triggers spontaneous condensation of formed peptidyl aldehydes with ε-amino groups of unmodified lysine residues or with vicinal peptidyl aldehydes [32].

LTQ biosynthesis is proposed to be similar to and as simple as TPQ (Figure 6). Autocatalytic hydroxylation of tyrosine precursor by molecular oxygen is copper(II)-dependent and results in formation of an *o*-dopaquinone (DPQ) intermediate [33]. The successive steps include cross-linking between ε-amino group of lysine residue and tyrosine ring at C-6 position, followed by the oxidation of formed *o*-quinol into *o*-quinone, oxidized by molecular oxygen.

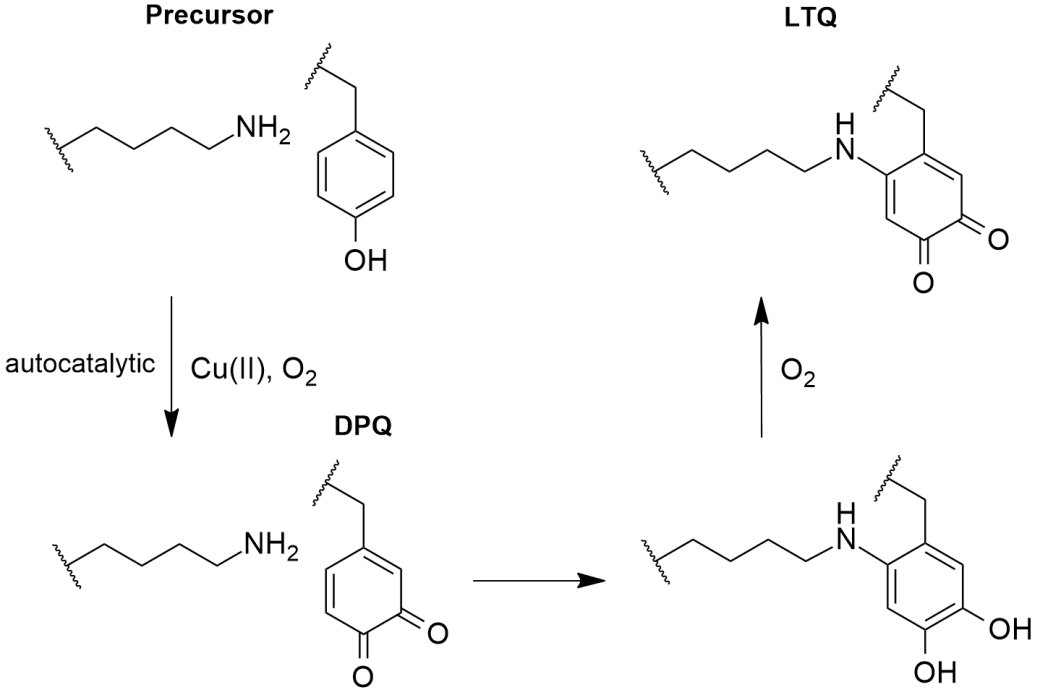

Figure 6. Biosynthesis of LTQ in lysyl oxidase.

Radical SAM enzymes with a SPASM domain

As mentioned above, one of the enzymes involved in PQQ biosynthesis is a radical S-adenosyl L-methionine (SAM) enzyme, PqqE. Enzymes of this type may be used to catalyze chemically difficult transformations, such as carbon-carbon [9] and thioether [34] bond formation, methylthiolation [35], oxidative decarboxylation [36] etc. This can be achieved through a radical mechanism that involves activation of a C-H bond in a substrate.

Radical SAM enzymes are a superfamily of enzymes that catalyze reductive cleavage of S-adenosyl L-methionine (SAM) into L-methionine and a 5′-deoxyadenosine radical (5′-dA•) in an uncoupled reaction. The hemolytic cleavage of SAM is initiated by $[4Fe\text{-}4S]^{1+}$ cluster (Figure 7). Upon exposure to substrate, the 5′-dA• radical abstracts a hydrogen, generally from a C-H bond, thus triggering the specific catalysis.

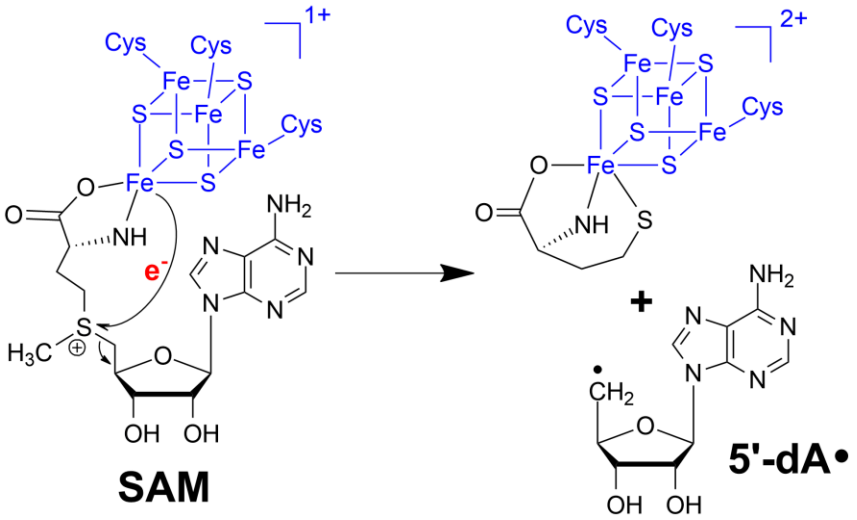

Figure 7. Reductive cleavage of S-adenosyl L-methionine (SAM) performed by $[4Fe\text{-}4S]^{1+}$ cluster within radical SAM enzyme, yielding the 5′-dA• radical.

Most radical SAM proteins contain a specific SAM-binding domain which represented by a partial $(\beta/\alpha)_6$ triose-phosphate isomerase (TIM) barrel fold [37, 38] (Figure 8). Within this domain, there are several motifs responsible for coordinating SAM. The most important among them is a highly conservative three-cysteine $CX_3CX\Phi C$ (Φ is for an aromatic residue) motif located in a loop following β1 strand. Cysteine residues from this motif ligate three irons from [4Fe-4S] cluster [39]; the fourth, "unique" iron is ligated to carboxylate and amino groups of L-methionine in SAM molecule [40]. Another notable conservative motif is Gly-Gly-Glu ("GGE") from β2 strand which forms hydrogen bonds with amino group of L-methionine in SAM, thus supporting ligation of SAM to the "unique" iron of the cluster [41]. Lastly, GXIXGXXE-motif (named after the corresponding sequence in BioB) located in β5 strand and non-conservative β6 structural motif provide hydrophobic stacking to adenine in SAM molecule [41]; also, β6 structural motif and the aromatic residue from the $CX_3CX\Phi C$ motif form hydrogen bonds with N1 and N6 of the adenine [37]. Residues responsible for coordinating ribose moiety in SAM molecule are in β4 and β5 strands [38].

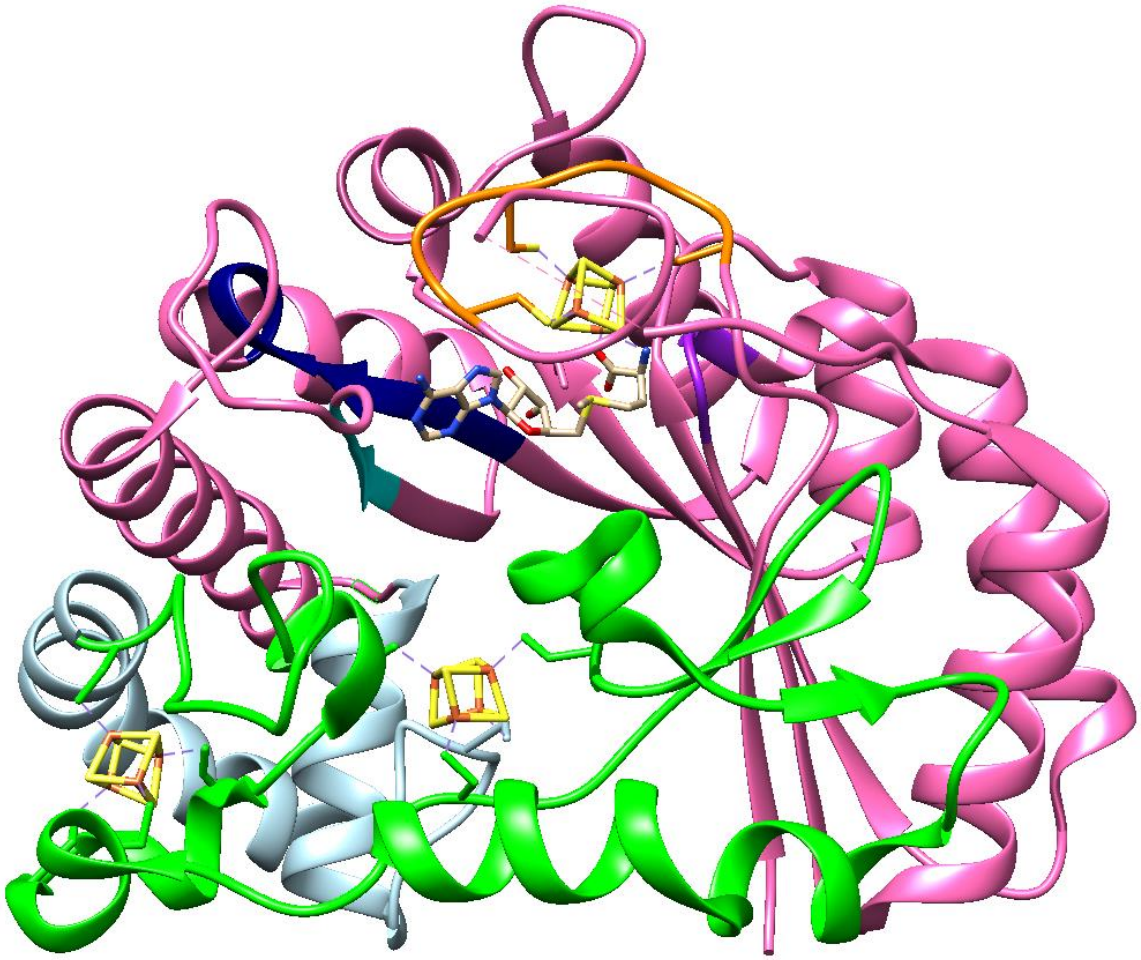

Figure 8. Crystal structure of a radical SAM enzyme anSME from *Clostridium perfringens* (PDB: 4K36). Radical SAM TIM-barrel domain is colored pink, SPASM domain (discussed below) is in green, elements that are not part of either domain are in light blue. Within radical SAM domain, $CX_3CX\Phi C$ motif is in orange, "GGE" motif is in purple, "GXIXGXXE" motif is in dark-blue, and the β6 motif is colored cyan. Within [4Fe-4S] clusters, Fe atoms are in orange and S atoms are in yellow. Cysteine residues ligating [4Fe-4S] clusters, and SAM molecule are represented as sticks.

Among radical SAM enzymes, there is a subfamily of enzymes shown to share a specific structure motif, called SPASM domain as a C-terminal extension to the basic radical SAM core. This domain contains two auxiliary [4Fe-4S] clusters ligated by a seven-cysteine $CX_{9\text{-}15}GX_4C$-gap-$CX_2CX_5CX_3C$-gap-C motif [42]. Although, the function of these clusters remains elusive, it is speculated that they may play a structural role or

might be involved in electron transfer, providing a sequential transport of an electron to the radical SAM cluster or an intermediate electron acceptor [43].

Enzymes of the SPASM subfamily (designated as TIGR08045) have been associated with posttranslational modifications of peptides [44, 45]. The name SPASM came as abbreviation from the biochemically characterized enzymes (Figure 9) that are involved in maturation of Subtilosin A (AlbA), PQQ (PqqE), Anaerobic Sulfatase (anSME) and Mycofactocin (MftC). AlbA catalyzes formation of three thioether bridges between sulfur atoms in cysteines and α-carbons in one threonine and two phenylalanines in Subtilosin precursor SboA [46, 47, 48]. PqqE, as discussed above, catalyzes the C-C bond formation between glutamate and tyrosine residues in PQQ precursor PqqA [9, 11]. AnSME (AtsB) catalyzes formation of formylglycine, an *in situ* arylsulfatase cofactor of anaerobic sulfatase AtsA, via two-step electron oxidation of corresponded cysteine or serine residue located in a conserved C(S)XPXR motif [49]. MftC catalyzes decarboxylation of the C-terminal tyrosine in mycofactocin precursor MftA [50, 51]. Currently, there are about 17000 sequences belonging to RS-SPASM protein subfamily, found in the InterPro database (designated as IPR023885).

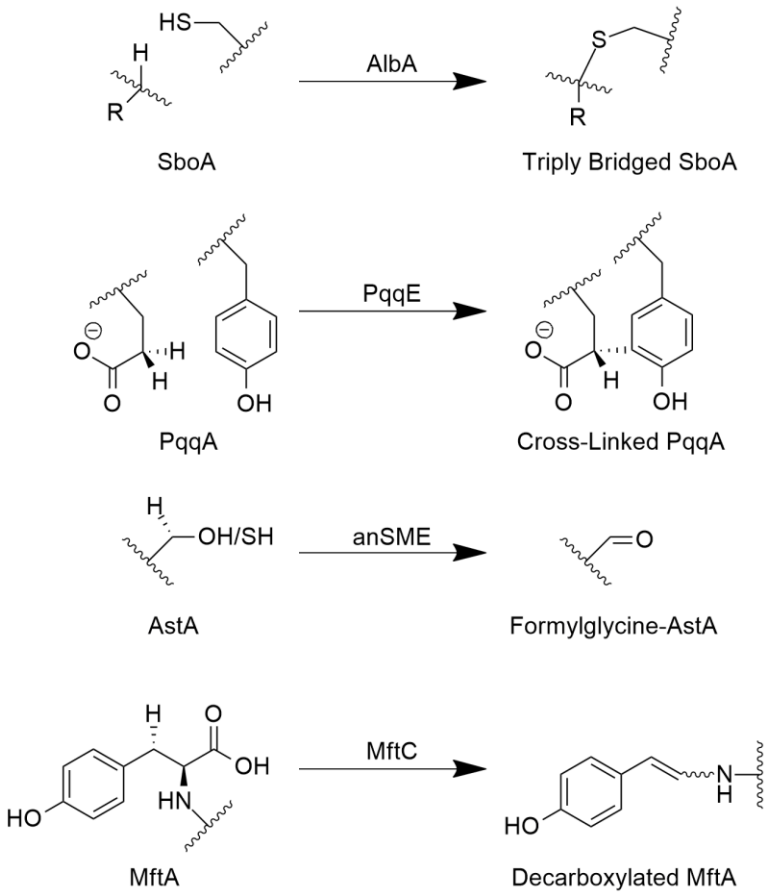

Figure 9. Reactions catalyzed by the characterized radical SAM enzymes from SPASM subfamily. For AlbA, formation of only one of three thioether bonds is shown. R is for side chain of Thr or Phe residue.

The only radical SAM protein with SPASM domain that has its structure characterized by X-ray crystallography at the moment is anSME from *Clostridium perfringens* [52] (Figure 8, PDB: 4K36). The solved structure confirmed the existence of two domains: parallel $(\beta/\alpha)_6$ partial TIM-barrel fold (radical SAM domain) at N-terminus (residues 3-234) and C-terminal SPASM domain with terminal α6′ helix which is not related to any domain; both domains are linked via α6a-helix.

Within the SAM-binding domain, it was shown that each of Cys15, Cys19 and Cys22 residues ligate one corresponding iron in one [4Fe-4S] cluster (RS-cluster) as part

of the conserved $CX_3CX\Phi C$ motif, and the "unique" iron is bound to the SAM molecule. In addition, Tyr21 residue was shown to form hydrogen bond with the SAM molecule. All the other motifs (GGE, GXIXGXXE, β6, and ribose motif) with expected interactions (discussed above) have also been found (Figure 10).

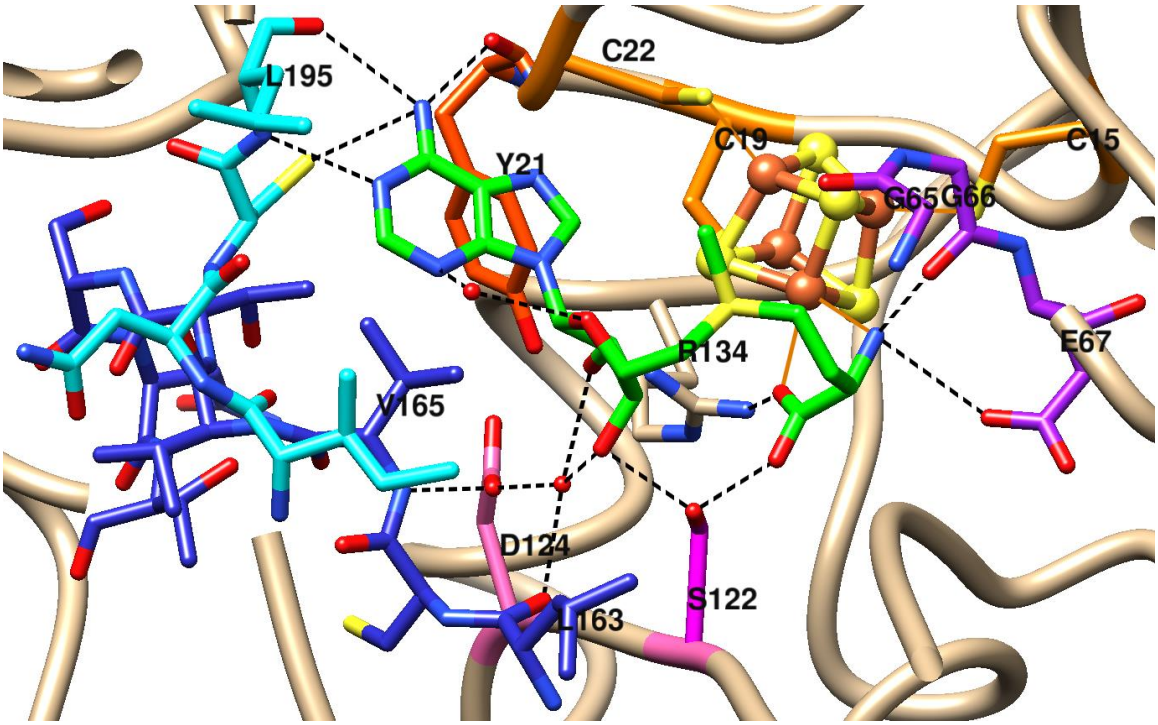

Figure 10. SAM-binding site of anSME from *C. perfringens*, represented in stick model. This includes [4Fe-4S] cluster-binding $CX_3CX\Phi C$ motif (C15, C19 and C22, orange, Y21, orange-red), "GGE" motif (G65, G66 and E67, purple), ribose motif (S122 and D124, pink) interacting with the ribose hydroxyl groups, "GXIXGXXE" motif (residues 163-170, blue), and the β6 motif (residues 192-195, cyan). Hydrogen bonds are shown as black dashed lines. Within [4Fe-4S] clusters, Fe atoms are in orange and S atoms are in yellow. Bound water molecules participating in hydrogen-bonding are shown as red spheres.

The C-terminal SPASM domain in anSME was shown to contain three secondary-structure elements: two anti-parallel β1′ and β2′ hairpins, conserved among TIGR04085 family, and a variable α2′ helix (Figure 11). Two auxiliary [4Fe-4S] clusters are coordinated by the seven-cysteine motif plus one upstream cysteine, all located in the

loops outside of the secondary-structure elements. The Aux I cluster is ligated by Cys255 (upstream residue, outside of the SPASM domain), Cys261, Cys276 (both from $CX_{9-15}GX_4C$-part) and Cys330 (the last cysteine from $CX_2CX_5CX_3C$-part); the α2′ helix shields the cluster from solvent. On the other hand, the Aux II cluster is bound to Cys317, Cys320, Cys326 (first three cysteines from $CX_2CX_5CX_3C$) and Cys348 (the final cysteine of the whole motif). The distances between the [4Fe-4S] clusters are the following: 12.9 Å between Aux I and Aux II, 16.9 Å between Aux I and RS and 26.7 Å between Aux II and RS [52].

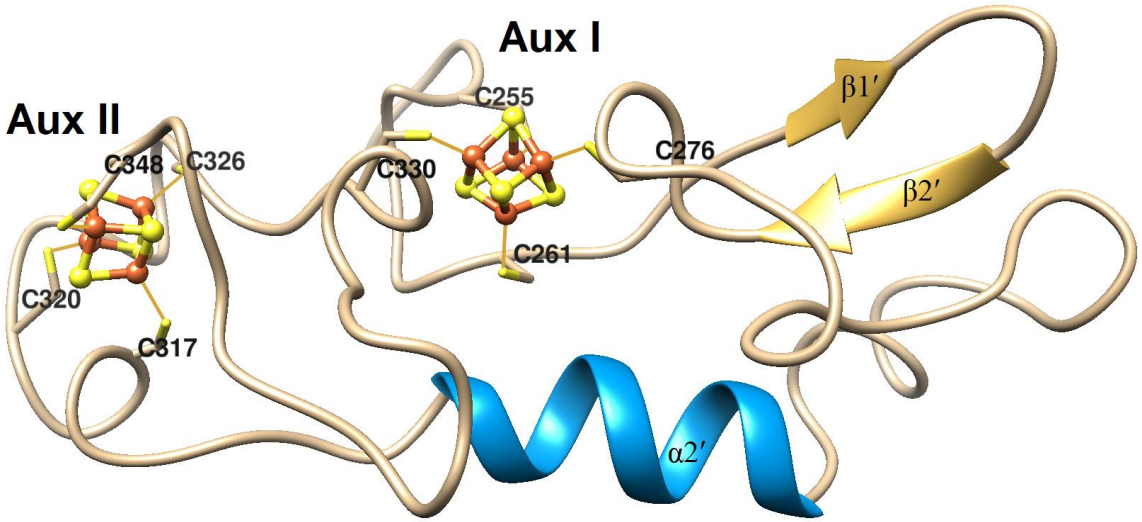

Figure 11. SPASM domain of anSME. α2′-helix is colored blue, β-hairpins are in light brown. Within Aux I and Aux II clusters, Fe atoms are in orange and S atoms are in yellow. Cysteine residues ligating [4Fe-4S] clusters are represented as sticks.

Mycofactocin biosynthetic pathway

As mentioned above, MftC is a radical SAM protein that belongs to the SPASM subfamily and catalyzes one of the steps of mycofactocin maturation.

The mycofactocin pathway was discovered in *Mycobacterium* family using Partial Phylogenetic Profiling method, in 2011 [44, 45]. The name “mycofactocin” has been

assigned because of the similarity of the novel gene cluster in *Mycobacterium* family to the biosynthetic clusters of PQQ redox cofactor and bacteriocin. Currently, the structure of mycofactocin has not been identified. It is speculated to be a small molecule with redox properties, serving as an electron carrier for short chain NAD-dependent dehydrogenases encoded upstream to the mycofactocin gene cluster [44, 53].

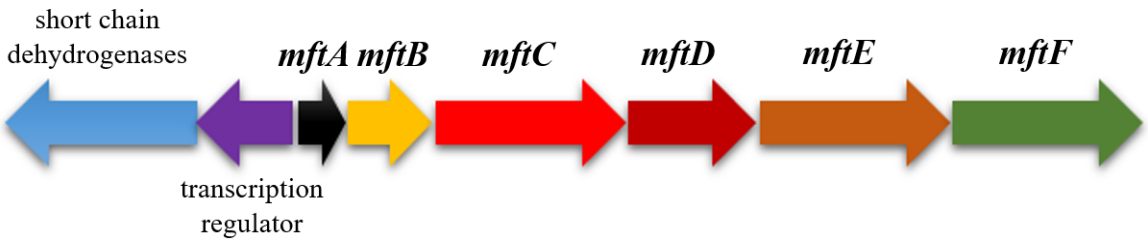

Figure 12. Mycofactocin gene cluster with near gene context from *Mycobacterium tuberculosis* (strain H37Rv).

The putative biosynthetic pathway of mycofactocin is suggested to be performed by gene products of the *mftABCDEF* operon (Figure 12), and these genes can only be found together. MftA is a short (30-78 amino acids) peptide precursor of mycofactocin, with a highly conserved C-terminal IDGXCGVY sequence. The initial step of the pathway is decarboxylation of MftA at a C-terminal tyrosine by MftC [50, 51]. This reaction occurs in presence of MftB, a small protein (about 100 amino acids) with no homologs. It was shown that MftB binds MftA precursor with nanomolar K_D and MftC enzyme with micromolar K_D [50], so it likely functions as a chaperone for the peptide precursor, acting similarly to PqqD chaperone towards PqqA [9, 11]. The product of this modification is shown to undergo amide bond cleavage by creatininase MftE, resulting in formation of a dipeptide product VY**, where Y** is a decarboxylated tyrosine residue that contains a double carbon-carbon bond [54]. The further steps of the pathway are not

known at the moment. The genes *mftD* (Rv0694 locus) and *mftF* (Rv0696 locus) encode for heme/flavin dehydrogenase (PF01070 Pfam superfamily) and glycosyltransferase (PF00535 Pfam superfamily), respectively [44, 53]. One can suggest that MftD acts after MftE, oxidizing the VY**, then MftF adds a glycosyl group to the resulting hydrophobic molecule, probably to facilitate its transport by any further enzymes on demand.

Mycofactocin biosynthetic pathway is critical for *M. tuberculosis* growth in cholesterol as a main carbon source: *mftC-F* (Rv0693-0696 loci) [55] and a gene encoding one of the upstream short chain dehydrogenases (Rv0687 locus) [56, 57] were shown to be essential for the cholesterol catabolism by *Mtb*. This fact can assure that the putative mycofactocin plays an important role in vital activity of *Mycobacterium* species. Therefore, investigations of this pathway may lead to the development of new drugs against tuberculosis, targeting the participants of the pathway.

CHAPTER TWO: MATERIALS AND METHODS

Expression and purification of MftC

The *mftC* gene (Uniprot: A0PM49) from *Mycobacterium ulcerans* Agy99 was cloned into the pET28a vector, using *NdeI* and *XhoI* restriction sites. The *mftC/pET28* plasmid construct was transformed into BL21(DE3) competent cell line, with pPH151 vector already transformed, carrying the *sufABCDSE* operon, and grown overnight. An overnight culture was used to inoculate 1 L of TB medium. The cells were grown at 37°C and 200 RPM until OD_{600} ~ 0.8-1.0, then were induced with sodium fumarate (0.75 g/L), $FeCl_3$ (50 μM) and 1 mM IPTG (isopropyl-β-thiogalactopyranoside). The cells were incubated anaerobically at 21°C overnight. The cell culture was centrifuged at 5500 g for 10 min and the pellet was transferred into the anaerobic chamber. The cells were suspended in 5-fold cell weight lysis buffer (50 mM Tris, 200 mM NaCl, 25 mM Imidazole, pH 7.6). CHAPS (1%), lysozyme (0.1%) and DNase (0.05 mg/g cell paste) were added to the suspension and stirred for 30 min at room temperature. The suspension was centrifuged at 30000 g for 15 min and transferred back into the anaerobic chamber. The supernatant was loaded onto a 5 mL His-Trap column (GE Life Sciences) in an ÄKTA Start FPLC system. The column was washed with 5 column volumes of lysis buffer (50 mM Tris, 200 mM NaCl, 25 mM Imidazole, pH 7.6), followed by elution buffer (50 mM Tris, 200 mM NaCl, 300 mM Imidazole, pH 7.6). The protein fraction was collected and buffer-exchanged to the storage buffer (50 mM HEPES, 100 mM

NaCl, pH 7.5) using PD-10 column. The solution was concentrated using Pall 30 kDa spin columns.

Reconstitution of MftC

All the operations were performed inside the anaerobic chamber. All reagents were transferred dry into the anaerobic chamber and dissolved in anaerobic water. Dithiothreitol (DTT) was added to a solution of the purified protein to final concentration of 10 mM. The solution was stirred for 30 min at 4°C. $FeCl_3$ was added to a 12-fold protein concentration, then the solution was stirred for 30 min at 4°C. Following the incubation, Na_2S was added to a 12-fold protein concentration, and solution incubated for 1 h at 4°C. The solution was then centrifuged at 16000 g for 2 min and the supernatant was buffer-exchanged into storage buffer (50 mM HEPES, 100 mM NaCl, pH 7.5) using PD-10 column. The final solution was concentrated using Pall 30 kDa spin columns, aliquoted, and stored at -80°C.

Determining concentration of MftC

Procedure for determining concentration of MftC was based on the previously published protocol [58]. To the 100 μL of MftC solution of unknown concentration, trichloroacetic acid (TCA) was added to final concentration of 10% (w/v). The mixture was incubated at -20°C for 30 min and centrifuged at 14000 g for 12 min. The pellet was washed two times with 500 μL of acetone, cooled at -20°C. The pellet was dried in air and dissolved in 500 μL of 8 M urea. Concentration of MftC was determined by

recording absorbance of the final solution at 280 nm, using molar extinction coefficient 39420 M^{-1}•cm^{-1} (assuming all cysteine residues were reduced). Value of molar extinction coefficient of polypeptide chain of MftC was calculated in ExPASy ProtParam web tool. Absorbance measurements were performed in Cary Bio 100 UV-visible spectrophotometer.

Quantification of iron and sulfide in MftC

Previously published protocols were used for quantification of iron and sulfide in MftC [59]. For iron quantification, 100 μL solution of ~25 μM MftC were prepared, and 10 μL of 3 M TCA were added to the solution. The mix was centrifuged at 14000 g for 12 min, and 330 μL of deionized water were added to the supernatant. Subsequently, 20 μL of 75 mM L-ascorbic acid, 20 μL of 10 mM 3-(2-pyridyl)-5,6-diphenyl-1,2,4-triazine-*p,p′*-disulfonic acid monosodium salt (ferrozine), and 20 μL of saturated sodium acetate were added to the solution. Concentration of iron was determined by recording absorbance of the final solution at 562 nm, using molar extinction coefficient 27900 M^{-1}•cm^{-1}. For sulfide quantification, 200 μL solution of ~12 μM MftC were prepared, and 600 μL of 1% (w/v) zinc acetate and 50 μL of 7% (w/v) sodium hydroxide were added subsequently to the solution. The mixture was inverted for several times and incubated for 15 min at room temperature. Subsequently, 150 μL of 0.1% (w/v) *N,N*-dimethylbenzene-1,4-diamine (DMPD) solution in 5 M HCl and 150 μL of 10 mM $FeCl_3$ solution in 1 M HCl were added to the mixture. The mixture was vortexed and incubated for 20 min at room temperature. Concentration of sulfide was determined by recording

absorbance of the final solution at 670 nm, using molar extinction coefficient 34500 M^{-1}•cm^{-1}. Corresponding reaction mixes with deionized water instead of MftC were used as blanks in both procedures. Absorbance measurements were performed using Cary Bio 100 UV-visible spectrophotometer.

SAM cleavage reactions

Reactions were performed in anaerobic chamber. All proteins were purified anaerobically. All the other reagents were transferred dry to the anaerobic chamber and dissolved in anaerobic deionized water. The reagents were mixed in the following order: reaction buffer (50 mM HEPES, 100 mM NaCl, pH 7.5), 1 mM sodium dithionite (DTH), 0,5, 1, 3, 5, 8 or 10 mM DTT, 1 mM SAM, 25 μM as-purified or reconstituted MftC. Aliquots of reaction mixes were taken at 0 min, 15 min, 30 min, 1 h, 2 h, 4 h, 6 h, 8 h, and 24 h, and trifluoroacetic acid (TFA) was added to final concentration of 1%. The mixes were centrifuged to remove precipitated MftC. The supernatant was diluted 10-fold and analyzed by reverse-phase chromatography on the Shimadzu Prominence-i LC-2030C HPLC using 4.6 × 50 mm C18 5 μm column (Restek, Bellefonte, PA, USA) and 5 mM sodium phosphate (pH 7.5, buffer A) and 0.1% TFA in water and acetonitrile as solvents. SAM and 5′-dA were tracked on the chromatogram monitoring absorbance at 254 nm. Concentrations of SAM and 5′-dA were calculated from integrations of the peak areas on the chromatogram. Initial rates of the reactions were determined from coefficients of trendlines fitting initial linear sections of 5′-dA accumulation curves. k_{cat} values were obtained by dividing the values of the reaction rates by MftC concentration.

Expression and purification of MftA

The undesignated *mftA* gene sequence from *Mycobacterium ulcerans* Agy99 was cloned into pET28HST vector using *NdeI* and *XhoI* restriction sites. The plasmid pET28HST was designed with His$_6$-tag added to the SUMO protein at N-terminus, and TEV protease cleavage site. When cloned into the *NdeI* restriction site, a Gly and His were added to the protein on the N-terminus after TEV cleavage. The *mftA/pET28HST* plasmid DNA was transformed into BL21 Star(DE3) (Invitrogen) competent cell line and grown overnight. The overnight culture was grown aerobically at 37°C in 4 mL of LB and then was used to inoculate LB medium. The cells were grown at 37°C and 200 RPM until OD_{600} ~ 0.6, then were induced with 1 mM IPTG (isopropyl-β-thiogalactopyranoside) and incubated at 21°C overnight. The cell culture centrifuged at 5500 g for 10 min, and the resulting pellet was suspended in 5-fold cell weight lysis buffer (50 mM Tris, 200 mM NaCl, 25 mM Imidazole, pH 7.6). The suspension was sonicated and centrifuged at 30000 g for 15 min. The supernatant was loaded onto a 5 mL HisTrap column (GE Life Sciences) using an ÄKTA FPLC system. The column was washed with 5 column volumes of lysis buffer (50 mM Tris, 200 mM NaCl, 25 mM Imidazole, pH 7.6), followed by elution buffer (50 mM Tris, 200 mM NaCl, 300 mM Imidazole, pH 7.6). The purified SUMO-MftA protein fraction was collected and buffer-exchanged to the sodium phosphate buffer (5 mM Na_2HPO_4, 1 mM TCEP, pH 7.5) using HiPrep 26/10 Desalting column (GE Life Sciences) and concentrated using Pall 10 kDa spin column. The TEV protease was added, and the solution was incubated at 4°C overnight, then centrifuged at 18000 g for 5 min. The supernatant was loaded onto semi-

prep 10 × 250 mm C4 5 μm reverse-phase column (Phenomenex) using Shimadzu Prominence-i LC-2030C HPLC using 5 mM sodium phosphate (pH 7.5, buffer A) and 5 mM sodium phosphate in 70% acetonitrile (pH 7.5, buffer B) as solvents. The MftA peptide fraction was collected and lyophilized overnight. The dry substance was transferred into the anaerobic chamber, dissolved in anaerobic deionized water, aliquoted, and stored at -80°C.

Expression and purification of GST-MftB

The *mftB* gene (Uniprot: A0PM48) from *Mycobacterium ulcerans* Agy99 was cloned into pGEX6p-1 vector (GE Life Sciences), using *BamHI* and *XhoI* restriction sites to obtain the GST-MftB fused protein. The *mftB/pGEX6p-1* plasmid construct was then transformed into BL21 Star(DE3) (Invitrogen) competent cell line and grown overnight. The overnight culture was grown aerobically at 37°C in 4 mL of LB and then was used to inoculate 1 L LB medium. The cells were grown at 37°C and 200 RPM until OD_{600} ~ 0.6, then were induced with 1 mM IPTG (isopropyl-β-thiogalactopyranoside) and incubated at 21°C overnight. The cell culture was centrifuged at 5500 g for 10 min and the resulting cell pellet was suspended in 5-fold cell weight lysis buffer (50 mM HEPES, 100 mM NaCl, 10% glycerol, pH 7.5). Lysozyme (0.1%) and DNase (0.05 mg/g cell paste) were added to the suspension and stirred for 10 min at room temperature. The suspension was sonicated and centrifuged at 30000 g for 15 min and transferred into the anaerobic chamber. The supernatant was loaded onto a 5 mL GSTrap column (GE Life Sciences) using an ÄKTA start FPLC system. The resin was washed with 5 volumes of lysis buffer,

followed by elution buffer (50 mM HEPES, 100 mM NaCl, 10% glycerol, 30 mM glutathione, pH 7.5). The protein fraction was collected, concentrated using Pall 10 kDa spin column and buffer-exchanged to the lysis buffer (50 mM HEPES, 100 mM NaCl, 10% glycerol, pH 7.5) using PD-10 column. The final solution was concentrated using Pall 10 kDa spin column, aliquoted, and stored at -80°C.

Labeling MftA with deuterium-labeled tyrosine

To obtain tyrosine deuterium-labeled variants of MftA, an overnight BL21 Star(DE3) culture containing the *mftA/pET28HST* plasmid was used to inoculate M9 minimal medium, containing all natural amino acids, and the deuterium-labeled tyrosine instead of natural tyrosine (each at 100 mg/L), glycerol (4 mL/L), Na_2HPO_4 (25 mM), KH_2PO_4 (25 mM), NH_4Cl (50 mM), Na_2SO_4 (5 mM), $MgSO_4$ (1 mM), $CaCl_2$ (100 μM), $FeCl_3$ (50 μM), pH 7.4. The growth and purification steps were performed as described above.

Labeling MftA with ^{13}C-labeled tyrosine

To obtain ^{13}C-labeled variants of MftA, an overnight *E. coli* RF4 culture containing the *mftA/pET28HST* construct was used to inoculate M9 minimal medium described above except with ^{13}C-labeled tyrosine instead of natural tyrosine (each at 100 mg/L). The growth and purification steps were performed as described above.

Deuterium-labeled MftA assay

Reactions were performed in anaerobic chamber. All the reagents were prepared as described above. The reagents were mixed in the following order: reaction buffer (50 mM HEPES, 100 mM NaCl, pH 7.5), 2 mM DTH, 8 mM DTT, 200 μM MftA, 200 μM GST-MftB, 400 μM SAM, 100 μM MftC. All the following steps were carried out as described above. The products of the reactions were tracked on the chromatogram monitoring absorbance at 260 nm and the corresponding fraction of 5′-dA was collected, lyophilized and dissolved in deionized water. The samples were analyzed by high resolution LC/MS.

MftA product purification assay

Reactions were performed in anaerobic chamber. All the reagents were prepared as described above. The reagents were mixed in the following order: reaction buffer (50 mM HEPES, 100 mM NaCl, pH 7.5), 2 mM DTH, 8 mM DTT, 300 μM MftA, 300 μM GST-MftB, 1 mM SAM, 300 μM MftC. Reactions were carried out at room temperature for 4 h. All the following steps were performed as described above. The products of the reactions were tracked on the chromatogram monitoring absorbance at 280 nm and the corresponding fraction of modified MftA was collected, lyophilized and dissolved in D_2O.

Nuclear Magnetic Resonance assay

All NMR spectra were recorded on a Bruker UltraShield 500/54 Plus spectrometer. Spectra were processed and analyzed in TopSpin 2.1 program (Bruker). All peptide NMR samples were prepared in D_2O. Suppression of H_2O signal was applied at a frequency of 2353.37 Hz. Signals were integrated and coupling constants were calculated in MestReNova 10.0.1 program (Mestrelab Research).

Site-directed mutagenesis

All the mutants were prepared using QuikChange protocol (Stratagene) with the Phusion polymerase. The *mftA/pET28HST* plasmids both with and without N-terminal methionine codon replaced to tryptophan (M1W) were used as template for PCR. The primers used for constructing the corresponding mutants are described in table 1. The mutants were sequence-verified and transformed into BL21 Star(DE3) competent cells.

Mutation	**Oligonucleotides**
M1W	Forward: TACTTCCAAGGCCATTGGGACCGTGAGACC Reverse: GGTCTCACGGTCCCAATGGCCTTGGAAGTA
Y30S	Forward: GCATGTGCGGCGTTTCCTAACTCGAGCAC Reverse: GTGCTCGAGTTAGGAAACGCCGCACATGC
Y30F	Forward: GCATGTGCGGCGTTTTCTAACTCGAG Reverse: CTCGAGTTAGAAAACGCCGCACATGC
Y30W	Forward: GCATGTGCGGCGTTTGGTAACTCGAG Reverse: CTCGAGTTACCAAACGCCGCACATGC
V29A	Forward: GCATGTGCGGCGCGTACTAACTCGAG Reverse: CTCGAGTTAGTACGCGCCGCACATGC

Table 1. Primers used to construct the mutants

MftA mutant reactions

Reactions were performed in anaerobic chamber. All proteins were purified anaerobically or buffer-exchanged to anaerobic buffer. All the other reagents were transferred dry to the anaerobic chamber and dissolved in anaerobic deionized water. The reagents were mixed in the following order: reaction buffer (50 mM HEPES, 100 mM NaCl, pH 7.5), 2 mM DTH, 8 mM DTT, 100 μM MftA, 100 μM GST-MftB, 1 mM SAM, 50 μM MftC. Reactions were carried out at room temperature for 18 h, then were centrifuged to remove any precipitated reagents and the supernatant was analyzed by reverse-phase chromatography on the Shimadzu Prominence-i LC-2030C HPLC using 4.6 × 250 mm C18 5 μm column (Phenomenex) and 5 mM sodium phosphate (pH 7.5, buffer A) and 5 mM sodium phosphate in 70% acetonitrile (pH 7.5, buffer B) as solvents. The products of the reactions were tracked on the chromatogram monitoring absorbance at 280 nm. The reaction mixture and starting MftA material samples were analyzed by high resolution LC/MS at the University of Colorado Anschutz Medical Campus Mass Spectrometry Facility.

CHAPTER THREE: RESULTS

MftC contains at least two [4Fe-4S] clusters

The *mftC* gene from *Mycobacterium ulcerans* was cloned and expressed in *Escherichia coli*. MftC protein was purified in anaerobic conditions to prevent unwanted oxidation of iron-sulfur clusters from by molecular oxygen. A fraction of the protein was used as it is (denoted "as-purified") while the other part was reconstituted with excess of iron and sulfur before usage (assigned "reconstituted"). The quality of the purification was monitored by SDS-PAGE (Figure 13A). The protein was estimated to be in a mass range of 40-42 kDa, which is consistent with the calculated molar mass of MftC. The UV-visible absorption spectrum of as-purified and reconstituted MftC (Figure 13B) shows a characteristic peak at 280 nm, and a specific "shoulder" at ~410 nm, which is characteristic for [4Fe-4S] cluster [60]. This "shoulder" is relatively larger in the case of reconstituted protein, consistent with the reconstituted MftC containing more [4Fe-4S] clusters per protein. The exact number of iron-sulfur clusters per polypeptide chain of MftC was determined through iron and sulfide quantification assays. From the analysis, we found that as-purified MftC contained 4.1 ± 0.1 equivalents of iron and 4.1 ± 0.1 equivalents of sulfide, which indicates presence of at least one [4Fe-4S] cluster. Reconstituted MftC was shown to have 10.0 ± 0.2 equivalents of iron and 8.1 ± 0.3 equivalents of sulfide, which indicates presence of at least two [4Fe-4S] clusters.

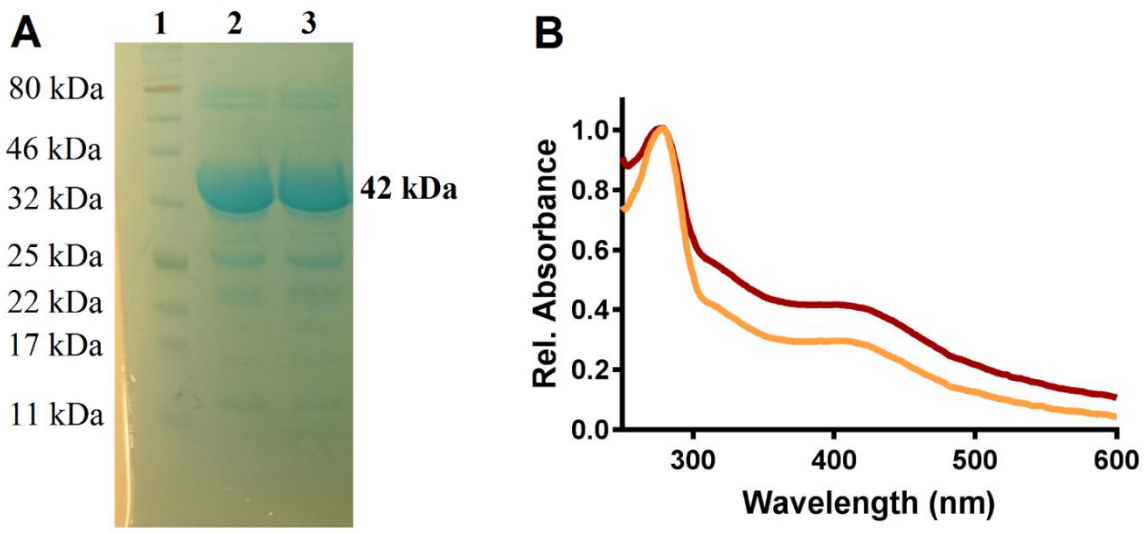

Figure 13. (A) Quality control of MftC purification by SDS-PAGE. Protein ladder (lane 1), as-purified MftC (lane 2), reconstituted MftC (lane 3); (B) UV-visible absorbance spectra of as-purified (orange) and reconstituted (brown) MftC.

For further confirmation of the presence of [4Fe-4S] clusters within the MftC, EPR analysis of the MftC was performed. MftC was treated with an excess of DTH in order to have all [4Fe-4S] clusters within MftC at +1 oxidation state. The local maximum in the CW spectrum is at g = 2.05, and the intensity goes through zero value at g = 1.93 (Figure 14). These values are consistent with the corresponding g-values of another RS-SPASM enzyme, PqqE (2.05 and 1.94, respectively) [61].

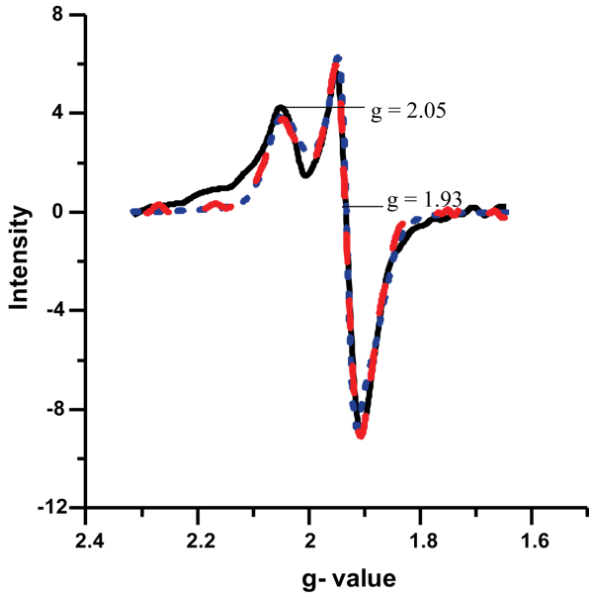

Figure 14. EPR spectra of reconstituted MftC. Background corrected spectrum at 25 K (solid black line), first derivative of the field-swept echo-detected spectrum at 10 K (dashed red line), simulation calculated in the Monmer program (dashed blue line) [50].

MftC can perform SAM cleavage in the presence of DTT as a reductant

MftC has been proposed to be a radical SAM protein [44] which means that this protein should catalyze the reductive cleavage of SAM. Cleavage of SAM requires DTH, because, as mentioned above, it reduces [4Fe-4S] cluster to +1 oxidation state, at which the cluster is able to perform the catalysis. We tested the ability of as-purified and reconstituted MftC to cleave SAM in the presence of DTH by monitoring formation of 5′-dA using reverse-phase HPLC. HPLC is often used to separate SAM and 5′-dA from each other [41]. In addition to DTH, MftC requires DTT to cleave SAM (Figure 15A). DTT is likely needed to reduce and reincorporate an iron cation into the radical SAM [4Fe-4S] cluster [62]. To determine the conditions under which MftC performs the cleavage with maximum efficiency, we varied the concentration of DTT from 0.5 to 10

mM in the reaction. The dependence of the reaction rate on DTT concentration fits Michaelis-Menten curve (Figure 15B). The optimal concentration of DTT appeared to be 8 mM, so it was used in further experiments. In addition, it was found that reconstituted MftC catalyzes SAM cleavage more efficiently (with k_{cat} = 0.058 min^{-1} for reconstituted versus 0.044 min^{-1} for as-purified MftC), probably because of full presence of radical SAM [4Fe-4S] clusters in the protein.

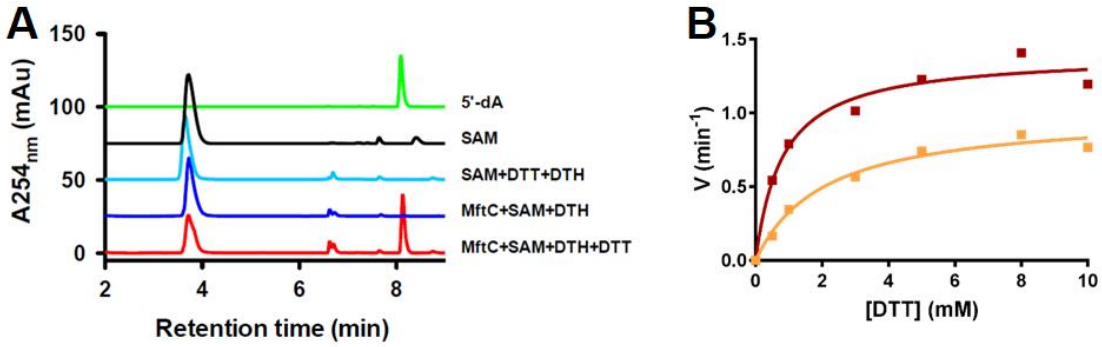

Figure 15. SAM cleavage performed by MftC depends on the presence of DTT. (A) HPLC chromatograms representing formation of 5′-dA during the reaction in the presence or absence of different reagents. Reconstituted MftC, SAM, DTH, and DTT (red), a mix with no DTT (blue), no MftC (cyan); SAM control (black), 5′-dA control (light green). [50] (B) Michaelis-Menten graph of SAM cleavage dependence on the DTT concentration, performed by as-purified (orange) and reconstituted (brown) MftC.

MftC catalyzes decarboxylation of the C-terminal tyrosine of MftA

It was proposed that MftA peptide is likely a potential substrate for MftC, and MftB, which is a small protein, likely participates in MftA modification [44]. To investigate the conditions of MftA modification by MftC, we used reverse phase HPLC. MftA starting material and a possible product of the modification might probably be separated in an HPLC column due to possible differences in their properties, such as mass and hydrophobicity. Mutant M1W MftA was constructed to increase intensity of the

absorbance at 280 nm, which helped to obtain a better signal on HPLC, because the molar extinction coefficient of wild-type MftA is 1490 M^{-1}•cm^{-1}, and incorporation of tryptophan increases it up to 6990 M^{-1}•cm^{-1} (calculated in ExPASy ProtParam web tool). HPLC analysis showed the appearance of a new peak at ~7.7 min when all the reagents including MftA, MftB, MftC, SAM, DTH and DTT were in the reaction mix, whereas in the controls where one of the reagents was lacking (ΔMftC, ΔSAM or ΔMftB) this peak did not appear (Figure 16). Formation of a new species represented by the new peak is consistent with the notion that MftC is modifying MftA. Notably, MftB was shown to be necessary for the reaction to proceed. As a small protein, it likely acts like a chaperone for MftA in the same manner as a small protein PqqD operates towards PqqA peptide during the modification by a radical SAM enzyme PqqE in PQQ biosynthetic pathway [9, 11]. We concluded that MftC catalyzes a certain modification of MftA in the presence of MftB. In all further experiments the reactions were performed with the following reagents: MftA variant substrate, MftB, reconstituted MftC, SAM, DTH and DTT, varying the concentrations of the reagents when needed.

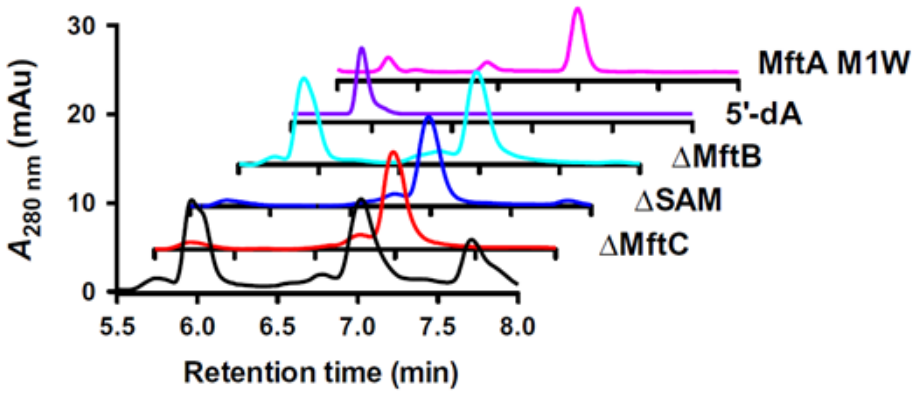

Figure 16. MftA modification by MftC depends on the presence of MftB. HPLC chromatograms showing appearance of a new peak at ~7.7 min during the reaction in the presence or absence of different reagents. M1W MftA, MftB, reconstituted MftC, SAM, DTH and DTT (black), a mix with no MftC (red), no SAM (blue), no MftC (cyan); 5′-dA control (purple), M1W MftA control (pink) [50].

To confirm that the new chemical reaction takes place, we analyzed the reaction mixes by high resolution LC/MS. By using LC/MS, we expected to detect a mass change on MftA, as a result of the reaction. Analysis of M1W MftA starting material showed a mass *m/z* = 1185.54 ($[M + 3H]^{3+}$, predicted 1185.54, Figure 17A). Analysis of the reaction mix showed a new species with a mass *m/z* = 1170.20 ($[M + 3H]^{3+}$, Figure 17B), which was never observed in control reaction mixes lacking any of the reagents. The difference between the starting material and the product appeared to be 46 Da, which was suggested to be a loss of 1C, 2O and 2H (with a possible new bond formation). Simulation of a mass spectrum data for M1W MftA without 1C, 2O and 2H is in good agreement with the obtained result.

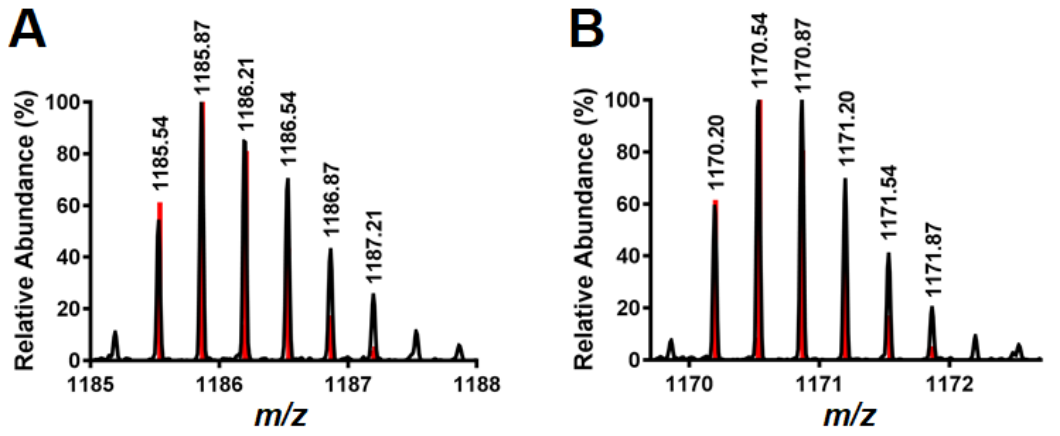

Figure 17. High-Resolution MS analysis of MftA modification. (A) Starting MftA material, (B) modified MftA material. Collected data for MS measurements are in black, simulated spectra for the corresponded $[M + 3H]^{3+}$ ions are in red.

To determine the location where the modification likely occurs, the $[M + 3H]^{3+}$ ions of both M1W MftA starting material and product were analyzed by tandem MS/MS. The *b*- and *y*-ions (N- and C-terminal polypeptide leftovers of an amide bound break, respectively) obtained from tandem MS/MS were used as a map to determine the position where the change occurred. We were unable to find b_{31}-ion and any *y*-ions in the product, (Figure 18B) that would be related to starting material (Figure 18A), whereas all the other *b*-ions that were also found in the starting material were presented, including b_{30}.

Figure 18. Tandem MS/MS analysis. (A) Starting MftA material, (B) Modified MftA material. Found *b*-fragments are in red, found *y*-fragments are in blue. Predicted fragments that were not found are in black [50].

From all this data, we concluded that modification of MftA is the decarboxylation at C-terminal tyrosine residue, with subtraction of two hydrogen atoms. Our first hypothesis was that this loss of 2H occurs due to the formation of C_α-C_β double bond at the C-terminal residue (Figure 19).

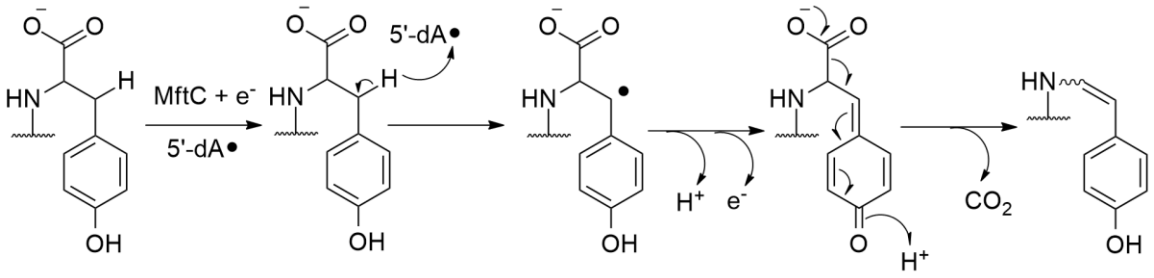

Figure 19. Initially proposed mechanism of the MftA modification by MftC.

5′-dA• radical abstracts hydrogen from C_β-position of C-terminal tyrosine

We proposed that 5′-dA• radical abstracts hydrogen from C_α- or C_β- position of tyrosine. To test this hypothesis and determine which hydrogen is abstracted, we labeled MftA peptide with tyrosine deuterated at C_α- and C_β- position, isolated 5′-dA formed in the process of reaction and analyzed by high-resolution LC/MS. We expected that 5′-dA would have a mass larger by 1 Da in case of a deuterium abstraction (5′-dA-D) instead of a natural hydrogen. M1W MftA peptide was labeled with ring-2,6-D_2, 2-D (at C_α) or 3,3-D_2 L-tyrosine (at C_β). According to the high-resolution LC/MS data (Figure S1A, S1B), the level of deuterated tyrosine incorporation into the peptide was ~40% in case of C_α and ~100% in C_β. The concentrations of all the reagents were set to minimize the amount of SAM consumed in order to increase the ratio of a deuterated 5′-dA presented versus natural 5′-dA, expecting 1:1 ratio. The HPLC fractions of 5′-dA were collected and analyzed by high resolution LC/MS. Analysis of a commercially produced 5′-dA (Sigma

Aldrich), serving as a negative control, showed a mass of *m/z* = 252.1098 ($[M + H]^+$, predicted 252.1091, Figure 20A), and simulation of 5′-dA-D spectrum predicts appearance of a mass *m/z* = 253.1154 ($[M + H]^+$, Figure 20B). After the reaction with C_α-deuterated tyrosine, 5′-dA had a signal of *m/z* = 252.1095 ($[M + H]^+$, Figure 20C), consistent with the negative 5′-dA control, whereas in case of C_β-deuterated tyrosine we were able to find ~30% of 5′-dA-D (*m/z* = 253.1158, $[M + H]^+$) in addition to the unlabeled 5′-dA (*m/z* = 252.1095, $[M + H]^+$, Figure 20D). From our findings, we can propose that it is the C_β-hydrogen of the C-terminal tyrosine that is abstracted by 5′-dA• radical as an initial step in the mechanism of MftA modification.

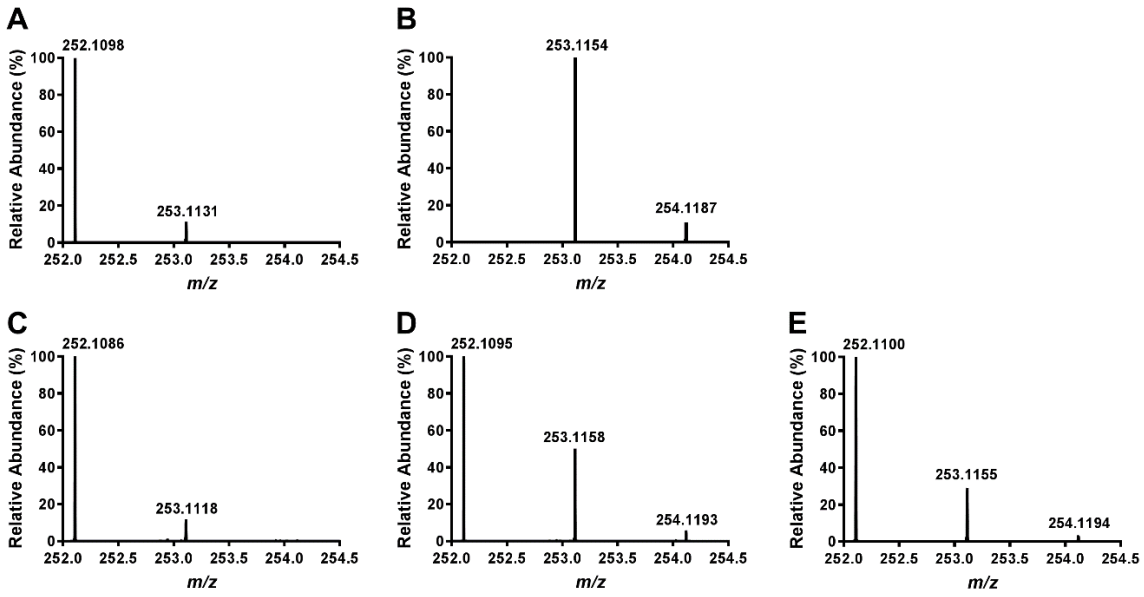

Figure 20. High-Resolution MS data of 5′-dA fractions purified by HPLC from reactions with deuterated labeled MftA variants. (A) 5′-dA control, (B) simulated spectra for 5′-dA with incorporation of one deuterium, (C) 5′-dA from the reaction with C_α-deuterated Tyr30 MftA, (D) with C_β-deuterated Tyr30 MftA, (E) with C_β-deuterated Val29 MftA variant.

MftA modification by MftC results in formation of two distinct products

To increase the quality of HPLC analysis, we changed analytical C18 HPLC column to a special C4 HPLC column constructed for peptide analysis. We noticed that in this case there are two peaks that appear on HPLC chromatogram during the reaction, found at ~14.3 (designated as "Product 1") and ~14.6 min (designated as "Product 2"), also the starting material was found at ~13 min (Figure 21A). From ~95% conversion of MftA starting material into the products, we observed ~90% of Product 1 and 10% Product 2. These peaks represent two different species with different UV-visible absorbance spectra patterns (Figure 21B): Product 1 has an absorbance maximum at ~278 nm, similarly to the starting material, whereas Product 2 has an absorbance maximum shifted to ~283 nm, with a specific "shoulder" at ~305 nm. Product 1 and product 2 were separated from each other by HPLC and analyzed by high-resolution LC/MS. Both products were found to have the same mass *m/z* = 1170.20 ($[M + 3H]^{3+}$, Figure S2), which indicates the loss of 1C, 2O and 2H in both cases. Considering this, we assumed that MftC catalyzed decarboxylation of MftA with formation of Product 1 and Product 2 as isomeric species.

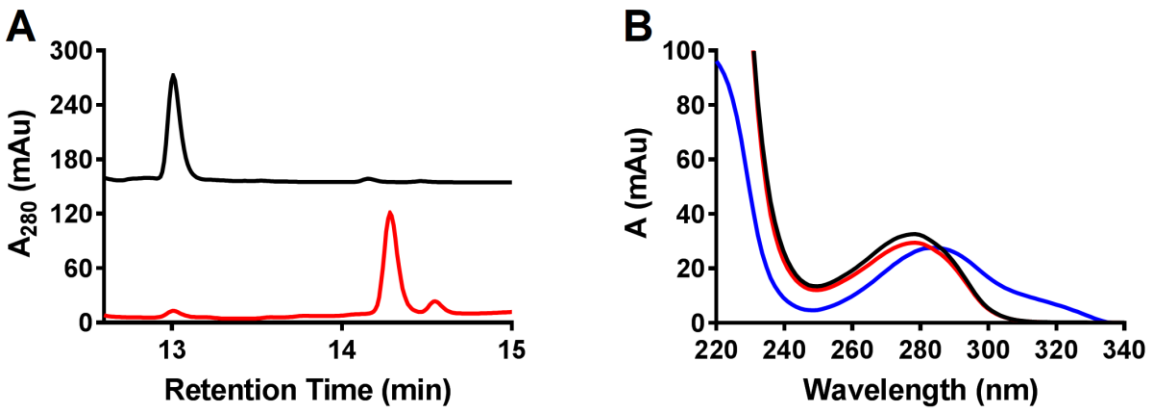

Figure 21. MftA modification by MftC results in formation of two distinct products, with the predominance of Product 1. (A) HPLC chromatograms of the reactions representing M1W MftA starting material (black) and its conversion into M1W Product 1 and M1W Product 2 (red). (B) UV-visible absorbance spectra of M1W MftA starting material (black), M1W Product 1 (red) and M1W Product 2 (blue).

MftA Product 1 does not contain an unsaturated carbon-carbon bond

To determine the exact structures of MftA modification products, we used ^{1}H NMR. M1W MftA starting material contains only three aromatic residues: C-terminal tyrosine, tryptophan (due to the M1W mutation), and histidine (purification leftover), therefore we anticipated that appearance of a carbon-carbon double bond would be detected in the corresponding region (δ ~ 4.50 to 7.00 ppm). ^{1}H NMR spectrum of M1W MftA starting material showed 11 signals of hydrogens in the aromatic region (δ ~ 5.50 to 8.50 ppm). Two doublets at δ ~ 6.70 and ~ 7.00 ppm belong to the tyrosine hydrogens, the tryptophan hydrogens are represented by two doublets at δ ~ 7.40 and 7.47 ppm, two triplets at δ ~ 7.05 and 7.15 and a singlet at δ ~ 6.65 ppm, and the last two singlets at δ ~ 7.11 and ~ 7.84 ppm represent the histidine hydrogens (Figure 22A). After the reaction, M1W MftA Product 1, as a predominant product, was purified by HPLC and analyzed by ^{1}H NMR. If the initially assumed mechanism is true, the substance after modification

would have a carbon-carbon double bond, so we expected to see a formation of two new doublets in the δ ~ 5.50 to 7.50 ppm region. Instead, we observed the appearance of two new singlets in this region, one at ~7.27 ppm and the other one at ~8.33 ppm, but no new doublets (Figure 22B). These results indicate that a carbon-carbon double bond is not formed. Moreover, it is likely that the new singlets are protected hydrogens from amide bonds on the peptide.

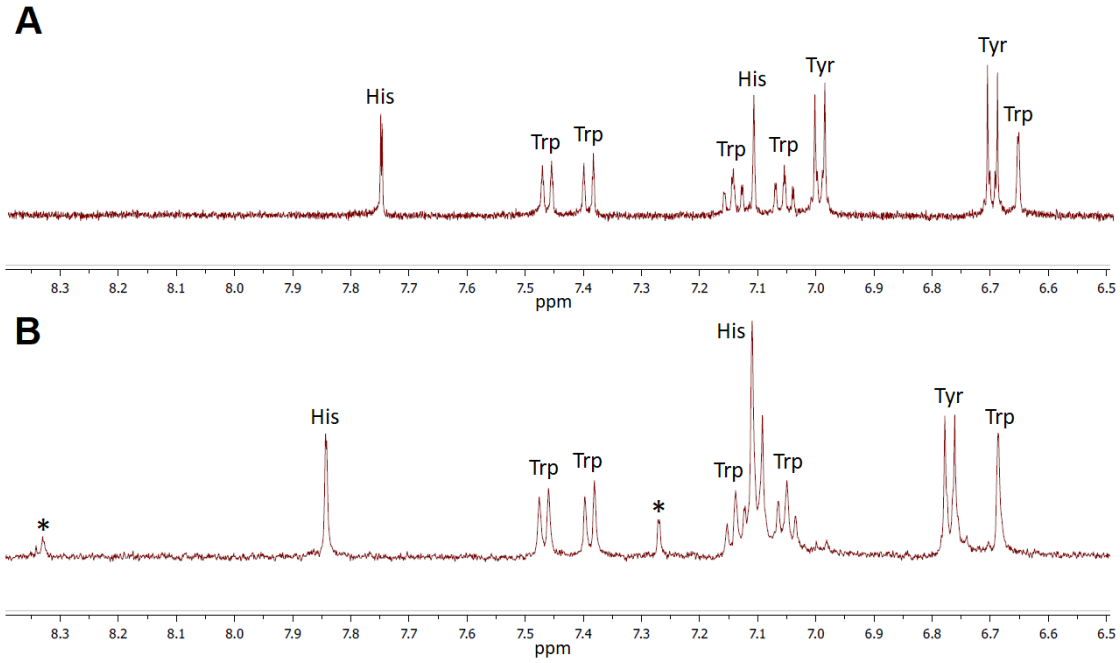

Figure 22. Aromatic region of ^{1}H NMR spectra of M1W MftA starting material (A), M1W Product 1 (B).

To validate this finding, we analyzed the structure of the Product 1 by ^{13}C NMR. For this approach, the sole natural tyrosine within the M1W MftA was substituted with $^{13}C_9$, ^{15}N-labeled tyrosine. The peptide was expressed in *E. coli* RF4(DE3) cell line to avoid degradation of labeled tyrosine, then purified by HPLC. According to the high-resolution LC/MS data (Figure S3A), the level of the labeled tyrosine incorporation into

the peptide was ~100%. NMR spectrum of the $^{13}C_9$-Tyr30 MftA showed 7 carbon signals, the most notable among them are δ ~ 57 and ~ 37 ppm representing C_α and C_β carbons, respectively, and δ ~ 177 ppm that belongs to a carbon from the carboxyl group (Figure 23A). The product of the reaction with the $^{13}C_9$-Tyr30 MftA was purified by HPLC and analyzed by high-resolution LC/MS. LC/MS analysis of the ^{13}C-Product 1 (Figure S3B) showed a mass lighter by 47 Da compared to the $^{13}C_9$-Tyr30 MftA, which indicated a loss of 1^{13}C, 2O and 2H. After the confirmation by LC/MS, the ^{13}C-Product 1 was analyzed by NMR. Based on the initially assumed mechanism, we expected to see the disappearance of a signal at δ ~ 177 ppm due to the decarboxylation at tyrosine. In case of an unsaturated bond formation, we would see a shift of the signals at δ ~ 37 and δ ~ 57 ppm into the δ ~ 100-130 ppm region. The resulting NMR spectrum of the ^{13}C-Product 1 showed that the signal at δ ~ 177 ppm disappeared, but the signals corresponding to C_α and C_β carbons did not shift significantly (Figure 23B). This data is not consistent with the formation of an unsaturated carbon-carbon bond in MftA. We could not predict the structure of the predominant product being limited by the original hypothesis, and the yield of the other product was too small to be analyzed by NMR.

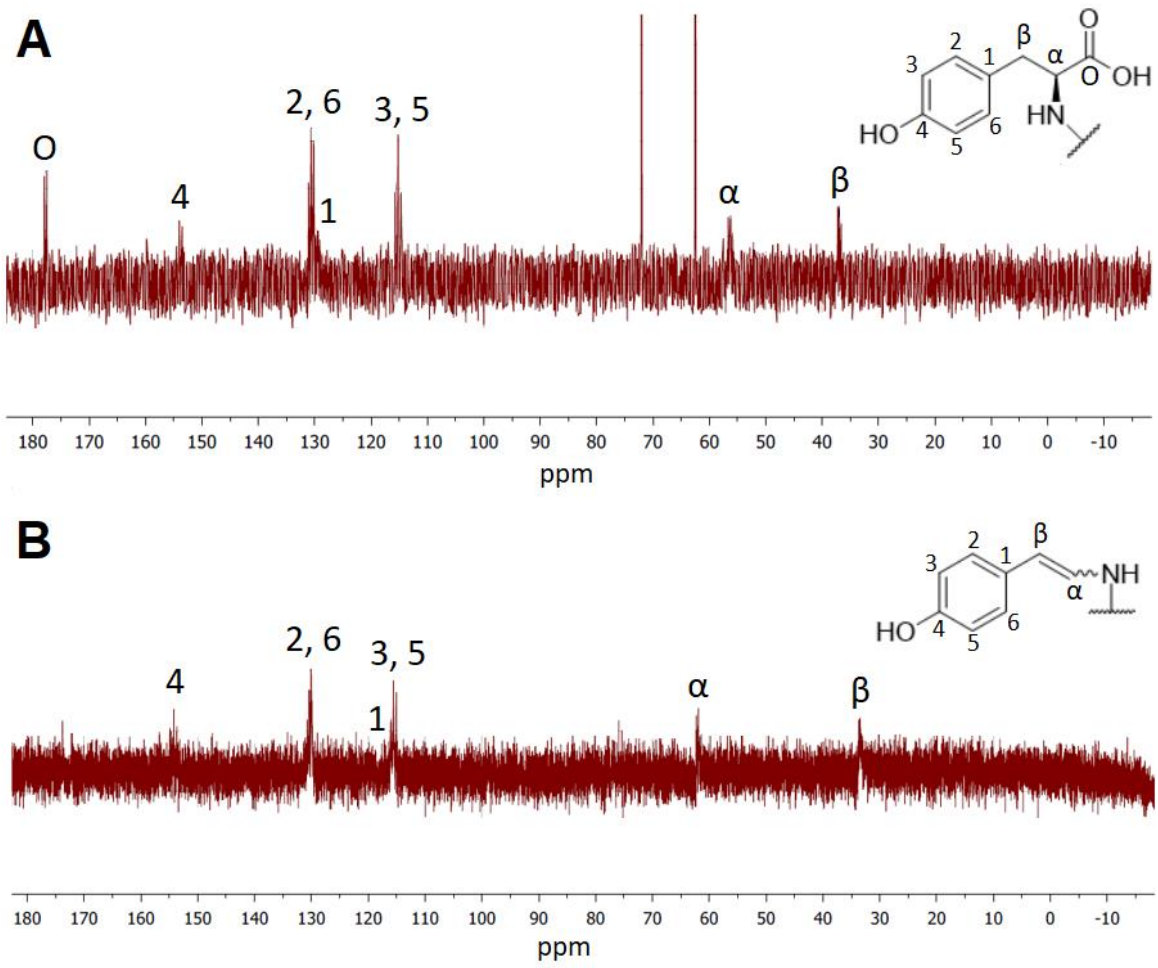

Figure 23. ^{13}C NMR spectra of $^{13}C_9$-Tyr30 MftA (A) and ^{13}C-Product 1 (B).

New hypothesis: MftC catalyzes cross-linking between Val29 and Tyr30 through an intermediate

Based on the data above, we devised a new hypothesis that the unsaturated bond containing species might not be a final product, but rather an intermediate that undergoes further cyclization with penultimate valine residue (Figure 24). According to predictions of ^{13}C NMR spectra for possible variants of the final product [63], we suggest that the cyclization likely occurs at C_α-position of tyrosine. In this case, MftA Product 1, as a

predominant product, might be the cyclized species that does not contain unsaturated bonds, whereas MftA Product 2, as a minor product, is probably the intermediate leftover with an unsaturated carbon-carbon bond.

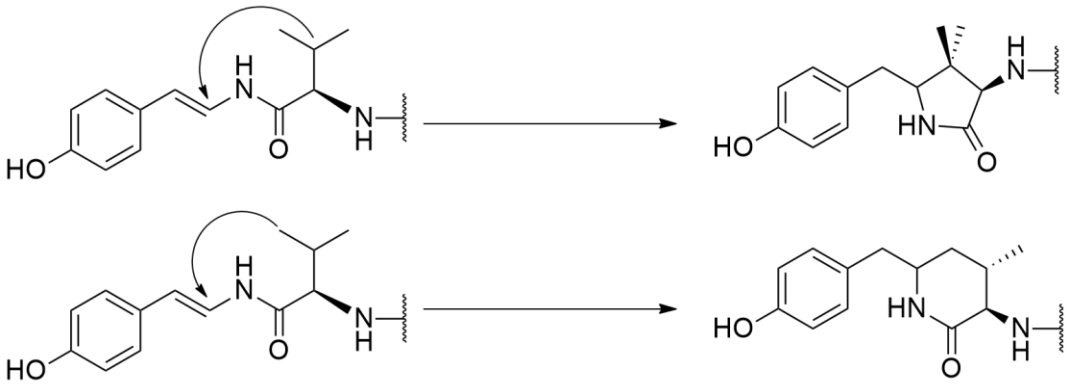

Figure 24. Possible transformations of the double-bond containing intermediate into various cross-linked final product variants.

To test if the penultimate valine was involved, we mutated it to alanine using the M1W MftA construct, and carried out reactions with MftC. HPLC analysis of the reaction with the V29A construct showed two product peaks, found at ~13.8 and ~14.2 min, along with the starting material at ~12.8 min (Figure 25A). Interestingly, from ~90% conversion of M1W V29A MftA starting material into the products, we observed ~10% of Product 1 and 90% Product 2, which is the opposite to the case of the reaction with the "natural" MftA peptide, however, this ratio varied from 10:90 to 40:60. UV-visible absorbance spectrum patterns of all the species were similar to the corresponding ones in case of M1W MftA: M1W V29A Product 1 showed an absorbance maximum at ~278 nm similar to the M1W V29A starting material, whereas M1W V29A Product 2 had an absorbance maximum at ~283 nm, with the same specific "shoulder" at ~305 nm (Figure 25B). Moreover, high-resolution LC/MS analysis showed a difference of 46 Da between

the M1W V29A starting material with *m/z* = 1176.18 ($[M + 3H]^{3+}$, Figure S4A) and M1W V29A Product 2 with *m/z* = 1160.85 ($[M + 3H]^{3+}$, Figure S4B), which represents a loss of 1C, 2O and 2H in a possible case of a decarboxylation with a double carbon-carbon bond formation, proposed for the intermediate.

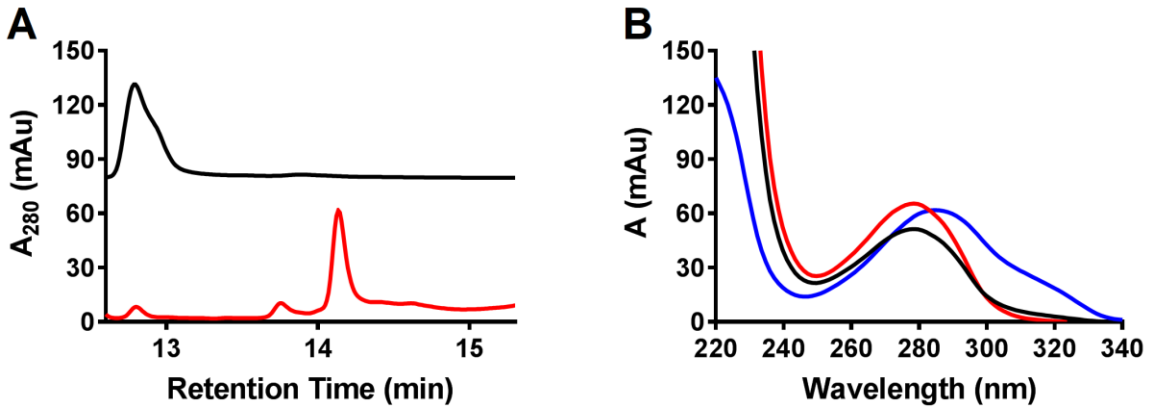

Figure 25. M1W V29A MftA modification by MftC leads to the predominance of Product 2. (A) HPLC chromatograms of the reactions representing M1W V29A MftA starting material (black) and its conversion into M1W V29A Product 1 and M1W V29A Product 2 (red). (B) UV-visible absorbance spectra of M1W V29A MftA starting material (black), M1W V29A Product 1 (red) and M1W V29A Product 2 (blue).

To determine the exact structure of M1W V29A Product 2, we used ^{1}H NMR. The aromatic region of ^{1}H NMR spectrum (δ ~ 5.50 to 8.50 ppm) of the M1W V29A starting material is proposed to be the same as the corresponding M1W MftA, because valine-to-alanine change has no significant effect on the tyrosine residue within the aromatic region. Therefore, we used ^{1}H NMR spectrum of M1W MftA starting material as a reference (Figure 26A). After the reaction with MftC, the formed M1W V29A Product 2 was purified by HPLC and analyzed by ^{1}H NMR. We noticed the appearance of two new doublets at δ ~ 6.27 and 7.25 ppm (Figure 26B) which represented formation of a double carbon-carbon bond. The *J*-coupling constant of the well-resolved doublet at

δ ~ 6.27 ppm was 14.7 Hz, which is specific for *trans*-configuration of the double bond. Considering the data obtained, we concluded that V29A mutation within MftA results in the accumulation of an intermediate containing a double carbon-carbon bond in a *trans*-configuration.

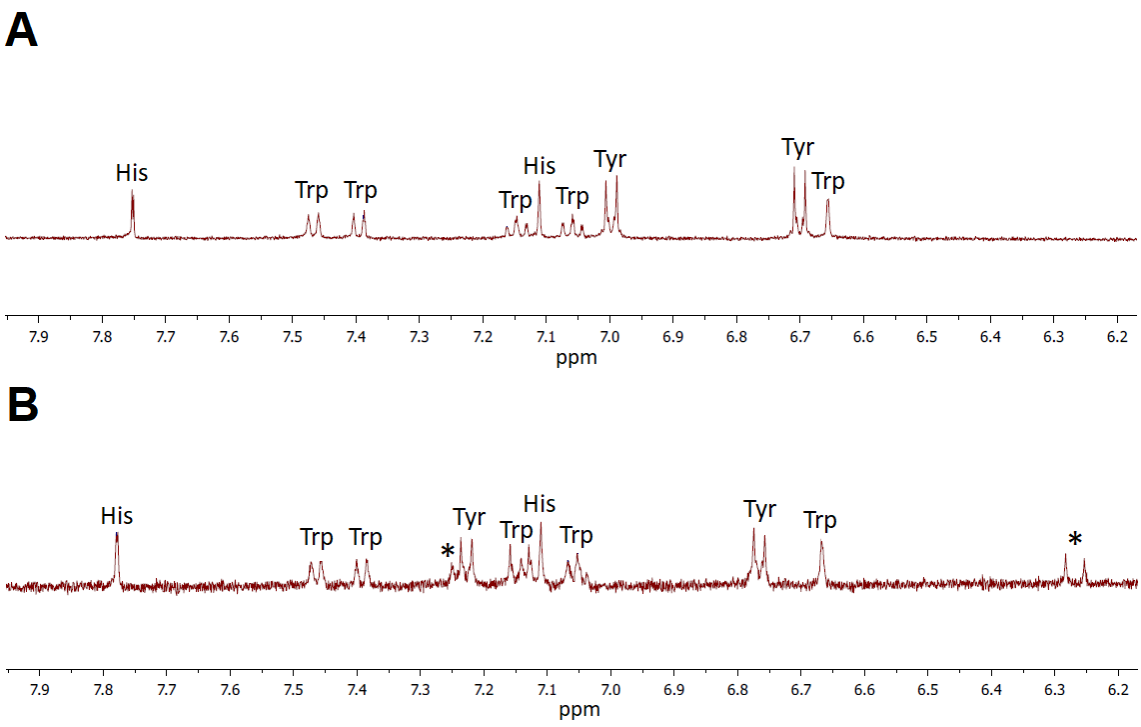

Figure 26. Aromatic region of ^{1}H NMR spectra of M1W MftA starting material (A) and M1W V29A Product 2 (B).

Based on the new hypothesis, the MftA Product 1 as a "final" product of MftC reaction is proposed to have a cross-linking carbon-carbon bond between C_{α} carbon of the C-terminal tyrosine and a carbon in the penultimate valine side chain. To test this, MftA was labeled with deuterated D_8-Val29. MftA contains three more valine residues within the peptide chain, V13, V18, and V21, therefore they were mutated to isoleucine residues as the amino acid with the closest similarity of side chain, in order to label V29

only. According to the high-resolution LC/MS data (Figure S5A), the level of D_8-valine incorporation into the peptide was ~50%. We would expect mass change of 47 Da during the reaction because of the deuterium loss instead of natural hydrogen. After the reaction with D_8-Val29 MftA, the product was 47 Da lighter with *m/z* = 1168.22 ($[M + 3H]^{3+}$, predicted 1168.22, Figure S5B), which indicated a loss of 1C, 2O, 1H and 1D. From this, we can conclude that the penultimate valine is involved in the reaction, possibly involved in a cross-linked product.

To determine which carbon was participating in the formation of a new bond, MftA was labeled with specifically deuterated 3-D-Val29. The V13I/V18I/V21I triple mutant MftA was used to label V29 only. Again, we would expect that after the reaction with MftC mass change of MftA would be 47 Da if the deuterium is abstracted from C_β-position, and 46 Da in case of abstraction of a natural hydrogen from C_α- or C_γ-position of the penultimate valine. According to the high-resolution LC/MS data (Figure S6A), the level of the 3-D labeled valine incorporation into the peptide was ~100%. After the reaction with 3-D-Val29 MftA, the product was 47 Da lighter, with *m/z* = 1165.88 ($[M + 3H]^{3+}$, predicted 1165.88, Figure S6B), as in the case of D_8-Val29 MftA, which indicated a loss of 1C, 2O, 1H and 1D. Based on this, we propose that a possible cross-linking occurs between the C-terminal tyrosine and the C_β-carbon of the penultimate valine.

The cross-linking is accompanied by an act of abstraction of a hydrogen from Val29, which is probably performed by 5′-dA• radical. It should be noted that when the penultimate valine was mutated to alanine, the corresponding Product 1 was a minor product, which means that the cross-linking may still occurred at a lower efficiency. This

is probably due to the relative instability of a primary radical compared to a tertiary one formed in the reaction with participation of alanine and valine side chains, respectively. To verify this, we collected the HPLC fraction of 5′-dA formed in the reaction with 3-D-Val29 MftA and analyzed it by high resolution LC/MS, as described above. We found ~12% of 5′-dA-D with *m/z* = 253.1155 ($[M + H]^+$) in addition to the unlabeled 5′-dA with *m/z* = 252.1100 ($[M + H]^+$, Figure 20E). From this finding, we propose that the final mechanism of MftA modification by MftC requires two equivalents of 5′-dA• radical to perform the whole catalysis proceeding through formation of the decarboxylated intermediate, resulting in the Val29-Tyr30 cross-linked final product (Figure 27).

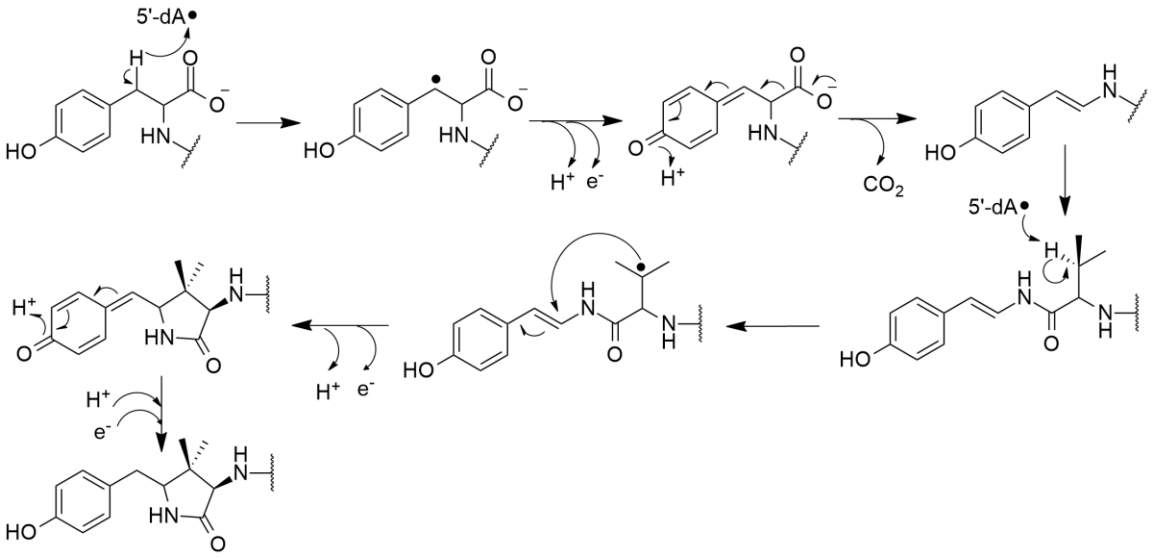

Figure 27. Revised mechanism of the MftA modification by MftC, including transformation of the intermediate into the cross-linked final product.

Labile proton at MftA C-terminus is required for the catalysis

As we proposed initially, the possible mechanism of MftA modification includes formation of a benzenone species from an intermediate radical (Figure 19). This step

involves a loss of a phenolic proton, which then is taken back during decarboxylation. That may be possible only if the proton is labile, e.g. exchanged easily. To test if the labile proton is required for the reaction to proceed, we mutated the C-terminal tyrosine in M1W MftA peptide to phenylalanine, serine and tryptophan. All the peptide variants were verified by high-resolution LC/MS (Figure S7). Reactions with the mutants were analyzed by HPLC with further analysis of UV-visible absorbance spectrum within 220-340 nm region.

At first, we substituted the C-terminal tyrosine by phenylalanine (Y30F), which is lacking the *p*-hydroxyl group and only contains a relatively inert hydrogen in its place. HPLC analysis of the reaction mix did not show any possible product with this mutant (Figure 28A). High-resolution LC/MS analysis also did not show appearance of any new species distinct from the M1W Y30F starting material with a mass *m/z* = 1180.20 ($[M + 3H]^{3+}$, predicted 1180.20). This data suggests that the *p*-hydroxyl group is an important component for MftC catalysis.

Next, we exchanged the C-terminal tyrosine to serine (Y30S) because it has a hydroxyl group similarly to tyrosine. HPLC analysis showed new species formed during the reaction with Y30S MftA. The starting material eluted at ~9.6 min, the possible product appeared at ~10.1 min, both shared the maximum absorbance at ~278 nm in the UV-visible absorbance spectrum (Figure 28B). In the LC/MS data for the reaction mix (Figure 28B) we could find the starting material with a mass 1160.19 ($[M + 3H]^{3+}$) and the corresponding decarboxylation product with loss of 46 Da (*m/z* = 1144.86, $[M + 3H]^{3+}$). In addition, we could observe appearance of a new species with *m/z* = 1150.19

([M + 3H]$^{3+}$), which was not shown by HPLC. Mass of this species is less by 30 Da than that of the Y30S starting material, indicating the loss of 1C, 1O, and 2H, which possibly represents transformation of the serine into glycine. We can conclude that MftC can perform both specific and even non-specific catalysis towards the peptide with a C-terminal serine, which is not a natural substrate for this enzyme.

Finally, we substituted the C-terminal tyrosine by tryptophan (Y30W) because its side chain has aromatic properties similar to tyrosine. In addition, a hydrogen bound to the indole nitrogen has a similar pK_a to tyrosine, as well. HPLC analysis showed appearance of two new peaks: one was eluted at ~10 min and the other one showed up at ~11.8 min (Figure 28C). The first peak eluted before the M1W Y30W starting material (at ~10.3 min). UV-visible absorbance spectrum of this species showed maximum absorbance at 260 nm and a "shoulder" at ~280 nm. Further analysis of the reaction by high-resolution LC/MS showed the starting material with a mass of *m/z* = 1193.21 ([M + 3H]$^{3+}$) and the corresponding decarboxylation product with loss of 46 Da (*m/z* = 1177.87, [M + 3H]$^{3+}$). Besides those two, a new peptide-based species with a mass of *m/z* = 1276.24 ([M + 3H]$^{3+}$) was found. This species is 249.1 Da heavier than the starting material. As we noticed, the mass of 5′-dA (251.1 Da) is close to that difference. This compound was likely formed in the process of a covalent binding of one 5′-dA molecule by the tryptophan residue, which would explain the loss of 2H to result in the exact mass match. In this case, the addition of 5′-dA is likely to be responsible for the appearance of the maximum absorbance at 260 nm, which is a characteristic pattern for adenosine. It should also be noticed that abundance levels of this species and the starting material in

the mass spectrum are almost the same, as well as the areas of the peaks on the HPLC chromatogram related to the major product and the starting material. In this case, we can match this peak to the corresponding heavy peptide species. Based on the data above, we propose that MftC can catalyze not only decarboxylation of a C-terminal tryptophan, which is not its natural substrate, but also a covalent addition of 5′-dA to this amino acid. However, the exact position of this addition remains unknown.

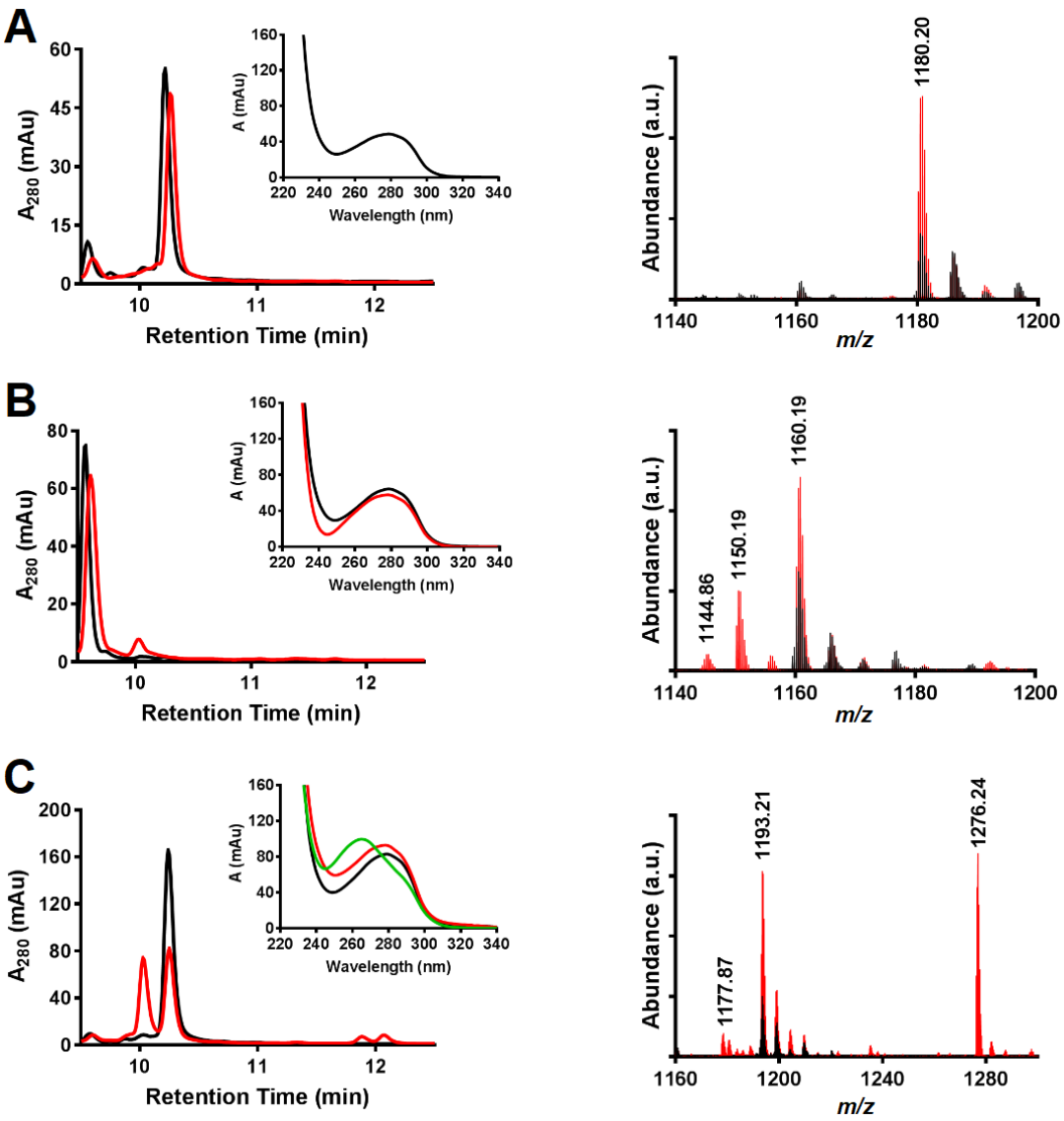

Figure 28. HPLC and high-resolution MS analysis of MftA mutants' modification by MftC. (A) M1W Y30F, (B) M1W Y30S, (C) M1W Y30W mutant. UV-visible absorbance spectra of the corresponding species are presented as insets. In all cases, the corresponding starting materials are colored in black, and the reacted peptide variants are in red. Green line in UV-vis represents spectrum for 5′-dA bound M1W Y30W peptide product.

CHAPTER FOUR: DISCUSSION AND SUMMARY

MftC is a radical SAM enzyme that contains at least two [4Fe-4S] clusters. Iron-sulfide quantification analysis of MftC from *M. ulcerans* Agy99 clearly showed the presence of two [4Fe-4S] clusters. The RS-cluster was ligated by the 30-$CX_3CX\Phi C$-37 motif; the C37A mutation in MftC resulted in loss of the cluster, and this mutant was not able to perform SAM cleavage (data not shown). Location of the other cluster was not determined precisely; its role in the catalysis remains unclear. Interestingly, the same RS-SPASM protein from different species can ligate different amounts of [4Fe-4S] clusters, two [61] or three [9]. Therefore, one cannot rule out the possibility for MftC to contain three [4Fe-4S] clusters. Nevertheless, the exact number of the auxiliary clusters ligated by MftC may not be critical for the catalysis.

Modification of MftA performed by MftC leads to the formation of two distinct isomeric products, with a ~90:10 ratio of Product 1 to Product 2. In case of using V29A MftA construct instead of the natural MftA, the ratio of the products was inverted. Since MftC is unlikely to perform the proper catalysis on the unnatural substrate, the reaction with the V29A MftA mutant was likely held at the halfway point of the entire modification. Consequently, Product 2 is probably an intermediate and Product 1 is the final product of the two-step modification of MftA. The intermediate was shown to contain a carbon-carbon double bond at the C-terminal tyrosine leftover. Simultaneous abstraction of an H-atom from the penultimate valine and vanishing of the carbon-carbon

double bond at the C-terminal tyrosine leftover is likely a result of cross-linking between these two residues. There is also a strong evidence that each step of this modification requires an equivalent of 5′-dA• radical.

Since modification of MftA by MftC is only the first step of the mycofactocin biosynthetic pathway, the product of this modification will serve as a starting material for any subsequent step. It is not known which of the two products may be a natural substrate for this. However, it has been shown recently that the creatininase MftE performs the second step of the pathway, resulting in formation of VY** species containing a carbon-carbon double bond [54]. That leads to the possibility that MftE used the intermediate Product 2 as its substrate, rather than the final Product 1. However, this reaction was performed *in situ* with MftC, and the product was never isolated as is. This leaves the opportunity to speculate that MftE could cleave both Products 1 and 2, resulting in formation of two distinct low molecular weight species. If this assumption is true, then the preferred substrate would be considered as a natural intermediate of the mycofactocin pathway. The LC/MS data provided in [54] showed presence of some ions derived from the double-bond containing variant of VY** which is an indirect evidence that Product 2 might be a natural product of the reaction performed by MftC. Further investigation of the low molecular weight products of MftE, including NMR analysis of their structures, would help to determine the natural product of MftC.

Also, MftC was able to react with Y30S and Y30W MftA constructs, performing its specific catalysis. According to the corresponding UV-visible spectroscopy data, it is likely that the specific products formed during the catalysis contain a cross-link with the

penultimate valine rather than a carbon-carbon double bond. However, the exact structures of these products were not determined. In addition to that, MftC implemented an unanticipated, non-specific catalysis on Y30S and Y30W, distinct for each construct, resulting in formation of non-specific products. Since these constructs are not natural substrates for MftC, it is unlikely that any of their corresponding products can undergo further modifications of the mycofactocin pathway properly. Therefore, these constructs have a potential to be used as possible inhibiting agents for this pathway, which might potentially be critical for vital activity of *Mycobacterium* species. Construction of new prospective drugs against *M. tuberculosis* could be based on these mutant variants of MftA peptide.

REFERENCES

1. Davidson, V. L. Structure and mechanism of tryptophylquinone enzymes. *Bioorganic Chemistry* **2005**, *33*, 159-170.
2. Mure, M. Tyrosine-derived quinone cofactors. *Acc. Chem. Res.* **2004**, *37*, 131-139.
3. Klinman, J. P.; Bonnot, F. Intrigues and Intricacies of the Biosynthetic Pathways for the Enzymatic Quinocofactors: PQQ, TTQ, CTQ, TPQ, and LTQ. *Chem. Rev.* **2014**, *114*, 4343-4365.
4. Kay, C. W.; Mennenga, B.; Görisch, H.; Bittl, R. Structure of the pyrroloquinoline quinone radical in quinoprotein ethanol dehydrogenase. *J. Biol. Chem.* **2006**, *281*, 1470-1476.
5. Davidson, V. L. Generation of protein-derived redox cofactors by posttranslational modification. *Mol. BioSyst.* **2011**, *7*, 29-37.
6. Hauge, J. G. Glucose Dehydrogenase of *Bacterium anitratum*: An Enzyme with a Novel Prosthetic Group. *J. Biol. Chem.* **1964**, *239*, 3630-3639.
7. Shen, Y. Q.; Bonnot, F.; Imsand, E. M.; RoseFigura, J. M.; Sjölander, K.; Klinman, J. P. Distribution and properties of the genes encoding the biosynthesis of the bacterial cofactor, pyrroloquinoline quinone. *Biochemistry* **2012**, *51*, 2265-2275.
8. Anthony, C. Pyrroloquinoline quinone (PQQ) and quinoprotein enzymes. *Antioxid. Redox Signal.* **2001**, *3*, 757-774.
9. Barr, I.; Latham, J. A.; Iavarone, A. T.; Chantarojsiri, T.; Hwang, J. D.; Klinman, J. P. Demonstration That the Radical S-Adenosylmethionine (SAM) Enzyme PqqE Catalyzes de Novo Carbon-Carbon Cross-linking within a Peptide Substrate PqqA in the Presence of the Peptide Chaperone PqqD. *J. Biol. Chem.* **2016**, *291*, 8877-8884.
10. Broderick, J. B.; Duffus, B. R.; Duschene, K. S.; Shepard, E. M. Radical S-adenosylmethionine enzymes. *Chem. Rev.* **2014**, *114*, 4229-4317.
11. Latham, J. A., Iavarone, A. T., Barr, I.; Juthani, P. V.; Klinman, J. P. PqqD is a novel peptide chaperone that forms a ternary complex with the radical S-adenosylmethionine protein PqqE in the pyrroloquinoline quinone biosynthetic pathway. *J. Biol. Chem.* **2015**, *290*, 12908-12918.
12. Wei, Q.; Ran, T.; Ma, C.; He, J.; Xu, D.; Wang., W. Crystal Structure and Function of PqqF Protein in the Pyrroloquinoline Quinone Biosynthetic Pathway. *J. Biol. Chem.* **2016**, *291*, 15575-15587.
13. Bonnot, F.; Iavarone, A. T.; Klinman, J. P. Multistep, eight-electron oxidation catalyzed by the cofactorless oxidase, PqqC: identification of chemical intermediates and their dependence on molecular oxygen. *Biochemistry* **2013**, *52*, 4667-4675.
14. Velterop, J. S.; Sellink, E.; Meulenberg, J. J.; David, S.; Bulder, I.; Postma, P. W. Synthesis of pyrroloquinoline quinone *in vivo* and *in vitro* and detection of an intermediate in the biosynthetic pathway. *J. Bacteriol.* **1995**, *177*, 5088-5098.
15. McIntire, W. S.; Wemmer, D. E.; Chistoserdov, A.; Lidstrom, M. E. A new cofactor in a prokaryotic enzyme: tryptophan tryptophylquinone as the redox prosthetic group in methylamine dehydrogenase. *Science* **1991**, *252*, 817-824.
16. Zhu, Z.; Davidson, V. L. Identification of a new reaction intermediate in the oxidation of methylamine dehydrogenase by amicyanin. *Biochemistry* **1996**, *35*, 8948-8954.

17. Pearson, A. R.; De La Mora-Rey, T.; Graichen, M. E.; Wang, Y.; Jones, L. H.; Marimanikkupam, S.; Agger, S. A.; Grimsrud, P. A.; Davidson, V. L.; Wilmot, C. M. Further insights into quinone cofactor biogenesis: probing the role of *mauG* in methylamine dehydrogenase tryptophan tryptophylquinone formation. *Biochemistry* **2004**, *43*, 5494-5502.
18. Williamson, H. R.; Sehanobish, E.; Shiller, A. M.; Sanchez-Amat, A.; Davidson, V. L. Roles of Copper and a Conserved Aspartic Acid in the Autocatalytic Hydroxylation of a Specific Tryptophan Residue during Cysteine Tryptophylquinone Biogenesis. *Biochemistry* **2017**, *56*, 997-1004.
19. Wang, Y.; Graichen, M. E.; Liu, A.; Pearson, A. R.; Wilmot, C. M.; Davidson, V. L. MauG, a novel diheme protein required for tryptophan tryptophylquinone biogenesis. *Biochemistry* **2003**, *42*, 7318-7325.
20. Yukl, E. T.; Liu, F.; Krzystek, J.; Shin, S.; Jensen, L. M.; Davidson, V. L.; Wilmot, C. M.; Liu, A. Diradical intermediate within the context of tryptophan tryptophylquinone biosynthesis. *Proc. Natl. Acad. Sci. U.S.A.* **2013**, *110*, 4569-4573.
21. Shin, S.; Abu Tarboush, N.; Davidson, V. L. Long-range electron transfer reactions between hemes of MauG and different forms of tryptophan tryptophylquinone of methylamine dehydrogenase. *Biochemistry* **2010**, *49*, 5810-5816.
22. Datta, S.; Mori, Y.; Takagi, K.; Kawaguchi, K.; Chen, Z. W.; Okajima, T.; Kuroda, S.; Ikeda, T.; Kano, K.; Tanizawa, K.; Mathews, F. S. Structure of a quinohemoprotein amine dehydrogenase with an uncommon redox cofactor and highly unusual crosslinking. *Proc. Natl. Acad. Sci. U.S.A.* **2001**, *98*, 14268-14273.
23. Okazaki, S.; Nakano, S.; Matsui, D.; Akaji, S.; Inagaki, K.; Asano, Y. X-ray crystallographic evidence for the presence of the cysteine tryptophylquinone cofactor in L-lysine ε-oxidase from *Marinomonas mediterranea*. *J. Biochem.* **2013**, *154*, 233-236.
24. Chacón-Verdú, M. D.; Campillo-Brocal, J. C.; Lucas-Elío, P.; Davidson, V. L.; Sánchez-Amat, A. Characterization of recombinant biosynthetic precursors of the cysteine tryptophylquinone cofactors of l-lysine-epsilon-oxidase and glycine oxidase from *Marinomonas mediterranea*. *Biochimica et Biophysica Acta* **2015**, *1854*, 1123-1131.
25. Takagi, K.; Yamamoto, K.; Kano, K.; Ikeda, T. New pathway of amine oxidation respiratory chain of *Paracoccus denitrificans* IFO 12442. *Eur. J. Biochem.* **2001**, *268*, 470-476.
26. Adachi, O.; Kubota, T.; Hacisalihoglu, A.; Toyama, H.; Shinagawa, E.; Duine, J. A.; Matsushita, K. Characterization of Quinohemoprotein Amine Dehydrogenase from *Pseudomonas putida*. *Biosci. Biotechnol. Biochem*. **1998**, *62*, 469-478.
27. Nakai, T.; Deguchi, T.; Frébort, I.; Tanizawa, K.; Okajima, T. Identification of genes essential for the biogenesis of quinohemoprotein amine dehydrogenase. *Biochemistry* **2014**, *53*, 895-907.
28. Janes, S. M.; Mu, D.; Wemmer, D.; Smith, A. J.; Kaur, S.; Maltby, D.; Burlingame, A. L.; Klinman, J. P. A new redox cofactor in eukaryotic enzymes: 6-hydroxydopa at the active site of bovine serum amine oxidase. *Science* **1990**, *248*, 981-987.

29. Janes, S. M.; Palcic, M. M.; Scaman, C. H.; Smith, A. J.; Brown, D. E.; Dooley, D. M.; Mure, M.; Klinman, J. P. Identification of topaquinone and its consensus sequence in copper amine oxidases. *Biochemistry* **1992**, *31*, 12147-12154.
30. Dubois, J. L.; Klinman, J. P. Mechanism of post-translational quinone formation in copper amine oxidases and its relationship to the catalytic turnover. *Archives of Biochemistry and Biophysics*, **2005**, *433*, 255-265.
31. Wang, S. X.; Mure, M.; Medzihradszky, K. F.; Burlingame, A. L.; Brown, D. E.; Dooley, D. M.; Smith, A. J.; Kagan, H. M.; Klinman, J. P. A crosslinked cofactor in lysyl oxidase: redox function for amino acid side chains. *Science* **1996**, *273*, 1078-1084.
32. Kagan, H. M.; Li, W. Lysyl oxidase: properties, specificity, and biological roles inside and outside of the cell. *Journal of Cellular Biochemistry* ***2003***, *88*, 660-672.
33. Moore, R. H.; Spies, M. A.; Culpepper, M. B.; Murakawa, T.; Hirota, S.; Okajima, T.; Tanizawa, K.; Mure, M. Trapping of a dopaquinone intermediate in the TPQ cofactor biogenesis in a copper-containing amine oxidase from *Arthrobacter globiformis*. *J. Am. Chem. Soc.* **2007**, *129*, 11524-11534.
34. Flühe, L.; Burghaus, O.; Wieckowski, B. M.; Giessen, T. W.; Linne, U.; Marahiel, M. A. Two [4Fe-4S] Clusters Containing Radical SAM Enzyme SkfB Catalyze Thioether Bond Formation during the Maturation of the Sporulation Killing Factor. *J. Am. Chem. Soc.* **2013**, *135*, 959-962.
35. Arragain, S.; Garcia-Serres, R.; Blondin, G.; Douki, T.; Clemancey, M.; Latour, J.-M.; Forouhar, F.; Neely, H.; Montelione, G. T.; Hunt, J. F.; Mulliez, E.; Fontecave, M.; Atta, M. Post-translational modification of ribosomal proteins: structural and functional characterization of RimO from *Thermotoga maritima*, a radical S-adenosylmethionine methylthiotransferase. *J. Biol. Chem.* **2010**, *285*, 5792-5801.
36. Layer, G.; Verfürth, K.; Mahlitz, E.; Jahn, D. Oxygen-independent Coproporphyrinogen-III Oxidase HemN from *Escherichia coli*. *J. Biol. Chem.* **2002**, *277*, 34136-34142.
37. Dowling, D. P.; Vey, J. L.; Croft, A. K.; Drennan, C. L. Structural diversity in the AdoMet radical enzyme superfamily. *Biochimica et Biophysica Acta* **2012**, *1824*, 1178-1195.
38. Vey, J. L.; Drennan, C. L. Structural insights into radical generation by the radical SAM superfamily. *Chem. Rev*. **2011**, *111*, 2487-2506.
39. Sofia, H. J.; Chen, G.; Hetzler, B. G.; Reyes-Spindola, J. F.; Miller, N. E. Radical SAM, a novel protein superfamily linking unresolved steps in familiar biosynthetic pathways with radical mechanisms: functional characterization using new analysis and information visualization methods. *Nucleic Acids Res.* **2001**, *29*, 1097-1106.
40. Walsby, C. J.; Ortillo, D.; Broderick, W. E.; Broderick, J. B.; Hoffman, B. M. An anchoring role for FeS clusters: chelation of the amino acid moiety of S-adenosylmethionine to the unique iron site of the [4Fe-4S] cluster of pyruvate formate-lyase activating enzyme. *J. Am. Chem. Soc*. **2002**, *124*, 11270-11271.
41. Nicolet, Y.; Drennan, C. L. AdoMet radical proteins – from structure to evolution – alignment of divergent protein sequences reveals strong secondary structure element conservation. *Nucleic Acids Res.* **2004**, *32*, 4015-4025.

42. Benjdia, A.; Subramanian, S.; Leprince, J.; Vaudry, H.; Johnson, M. K.; Berteau, O. Anaerobic sulfatase-maturating enzyme – a mechanistic link with glycyl radical-activating enzymes? *FEBS Journal* **2010**, *277*, 1906-1920.
43. Lanz, N. D.; Booker, S. J. Auxiliary iron-sulfur cofactors in radical SAM enzymes. *Biochimica et Biophysica Acta* **2015**, *1853*, 1316-1334.
44. Haft, D. H. Bioinformatic evidence for a widely distributed, ribosomally produced electron carrier precursor, its maturation proteins, and its nicotinoprotein redox partners. *BMC Genomics* **2011**, 12:21
45. Haft, D. H.; Basu, M. K. Biological systems discovery *in silico*: radical S-adenosylmethionine protein families and their target peptides for posttranslational modification. *J. Bacteriol.* **2011**, *193*, 2745-2755.
46. Flühe, L.; Knappe, T. A.; Gattner, M. J.; Schäfer, A.; Burghaus, O.; Linne, U.; Marahiel, M. A. The radical SAM enzyme AlbA catalyzes thioether bond formation in subtilosin A. *Nat. Chem. Biol.* **2012**, *8*, 350-357.
47. Zhang, Q.; Yu, Y. Thioether crosslinkages created by a radical SAM enzyme. *ChemBioChem* **2012**, *13*, 1097-1099.
48. Benjdia, A.; Guillot, A.; Lefranc, B.; Vaudry, H.; Leprince, J.; Berteau, O. Thioether bond formation by SPASM domain radical SAM enzymes: C_α H-atom abstraction in subtilosin A biosynthesis. *Chem. Commun. (Camb)* **2016**, *52*, 6249-6252.
49. Fang, Q.; Peng, J.; Dierks, T. Post-translational formylglycine modification of bacterial sulfatases by the radical S-adenosylmethionine protein AtsB. *J. Biol. Chem.* **2004**, *279*, 14570-14578.
50. Khaliullin, B.; Aggarwal, P.; Bubas, M.; Eaton, G. R.; Eaton, S. S.; Latham, J. A. Mycofactocin biosynthesis: modification of the peptide MftA by the radical S-adenosylmethionine protein MftC. *FEBS Letters* **2016**, *590*, 2538-2548.
51. Bruender, N. A.; Bandarian, V. The Radical S-Adenosyl-l-methionine Enzyme MftC Catalyzes an Oxidative Decarboxylation of the C-Terminus of the MftA Peptide. *Biochemistry* **2016**, *55*, 2813-2816.
52. Goldman, P. J.; Grove, T. L.; Sites, L. A.; McLaughlin, M. I.; Booker, S. J.; Drennan, C. L. X-ray structure of an AdoMet radical activase reveals an anaerobic solution for formylglycine posttranslational modification. *Proc. Natl. Acad. Sci. U.S.A.* **2013**, *110*, 8519-8524.
53. Haft, D. H.; Pierce, P. G.; Mayclin, S. J.; Sullivan, A.; Gardberg, A. S.; Abendroth, J., Begley, D. W.; Phan, I. Q.; Staker, B. L.; Myler, P. J.; Marathias, V. M.; Lorimer, D. D.; Edwards, T. E. Mycofactocin-associated mycobacterial dehydrogenases with non-exchangeable NAD cofactors. *Sci. Rep.* **2017**, *7*, 41074.
54. Bruender, N. A.; Bandarian, V. The Creatininase Homolog MftE from *Mycobacterium smegmatis* Catalyzes a Peptide Cleavage Reaction in the Biosynthesis of a Novel Ribosomally Synthesized Post-translationally Modified Peptide (RiPP). *J. Biol. Chem.* **2017**, *292*, 4371-4381.
55. Griffin, J. E.; Gawronski, J. D.; Dejesus, M. A.; Ioerger, T. R.; Akerley, B. J.; Sassetti, C. M. High-resolution phenotypic profiling defines genes essential for mycobacterial growth and cholesterol catabolism. *PLoS Pathog.* **2011**, *7*, e1002251.

56. Sassetti, C. M.; Rubin, E. J. Genetic requirements for mycobacterial survival during infection. *Proc. Natl. Acad. Sci. U.S.A.* **2003**, *100*, 12989-12994.
57. Wipperman, M. F.; Sampson, N. S.; Thomas, S. T. Pathogen roid rage: cholesterol utilization by *Mycobacterium tuberculosis*. *Crit. Rev. Biochem. Mol. Biol.* **2014**, *49*, 269-293.
58. Nakai, T.; Ito, H.; Kobayashi, K.; Takahashi, Y.; Hori, H.; Tsubaki, M.; Tanizawa, K.; Okajima, T. The Radical S-Adenosyl-L-methionine Enzyme QhpD Catalyzes Sequential Formation of Intra-protein Sulfur-to-Methylene Carbon Thioether Bonds. *J. Biol. Chem.* **2015**, *290*, 11144-11166.
59. Schramma, K. R.; Bushin, L. B.; Seyedsayamdost, M. R. Structure and biosynthesis of a macrocyclic peptide containing an unprecedented lysine-to-tryptophan crosslink. *Nat. Chem.* **2015**, *7*, 431-437.
60. Johnson, M. K.; Robinson, A. E.; Thomson, A. J. in *Iron-sulfur Proteins*; Spiro, T. G., Ed.; Wiley-Interscience: New York, 1982; pp 367-406.
61. Wecksler, S. R.; Stoll, S.; Tran, H.; Magnusson, O. T.; Wu, S.-p.; King, D.; Britt, R. D.; Klinman, J. P. Pyrroloquinoline Quinone Biogenesis: Demonstration That PqqE from *Klebsiella pneumoniae* Is a Radical S-Adenosyl-L-methionine Enzyme. *Biochemistry* **2009**, *48*, 10151-10161.
62. Padovani, D.; Thomas, F.; Trautwein, A. X.; Mulliez, E.; Fontecave, M. Activation of Class III Ribonucleotide Reductase from *E. coli*. The Electron Transfer from the Iron-Sulfur Center to S-Adenosylmethionine. *Biochemistry* **2001**, *40*, 6713-6719.
63. Banfi, D.; Patiny, L. www.nmrdb.org: Resurrecting and processing NMR spectra on-line. *Chimia*, **2008**, *62*, 280-281.

APPENDIX A

Supplemental Information

For all the figures below, collected data for MS measurements are in black, simulated spectra for corresponded $[M + 3H]^{3+}$ ions are in red.

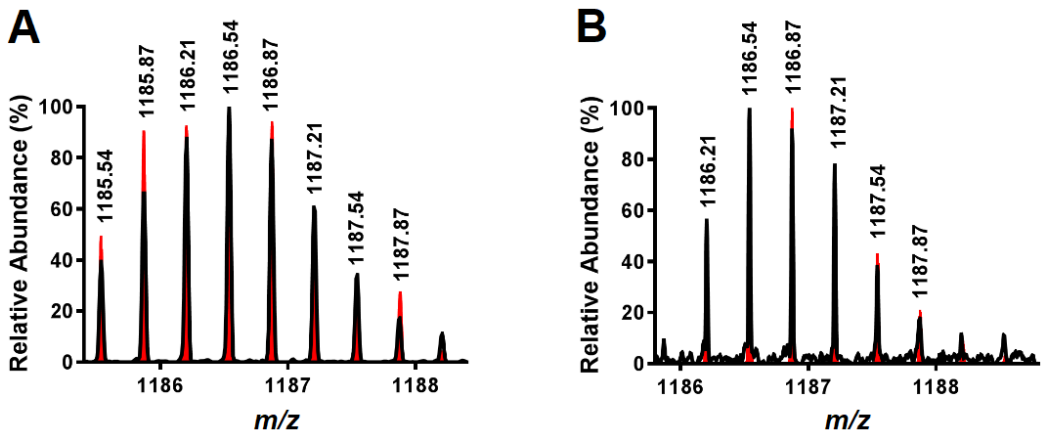

Figure S1. High-Resolution MS analysis of M1W MftA starting materials, labeled by (A) ring-2,6-D_2, 2-D tyrosine, (B) 3,3-D_2 tyrosine.

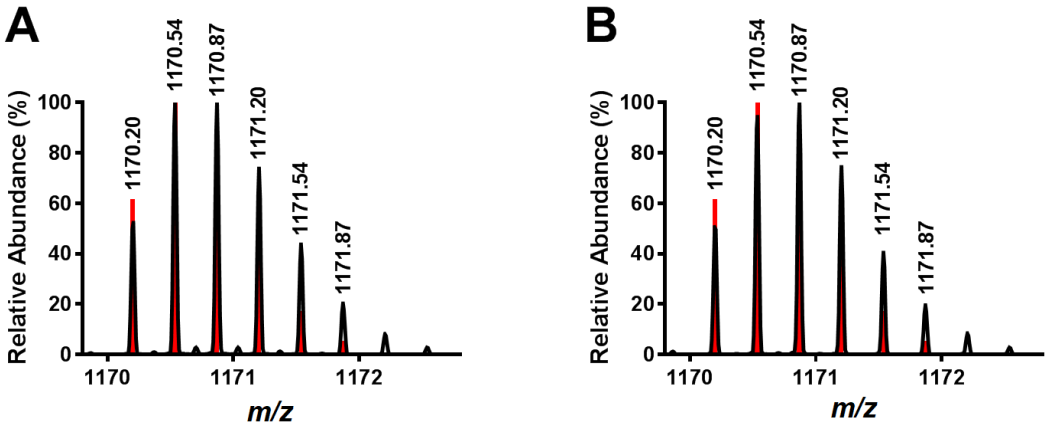

Figure S2. High-Resolution MS analysis of M1W reaction products. (A) M1W Product 1, (B) M1W Product 2.

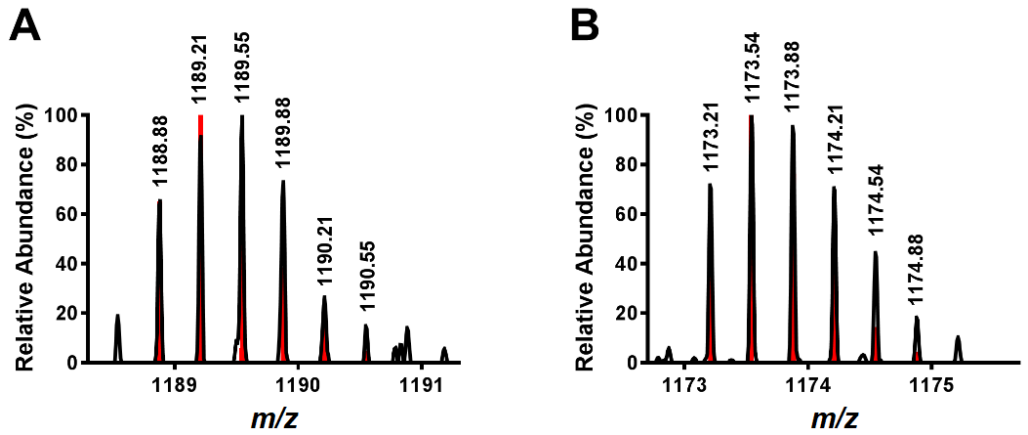

Figure S3. High-Resolution MS analysis of $^{13}C_9$-Tyr30 MftA modification. (A) $^{13}C_9$-Tyr30 MftA starting material, (B) ^{13}C-Product 1.

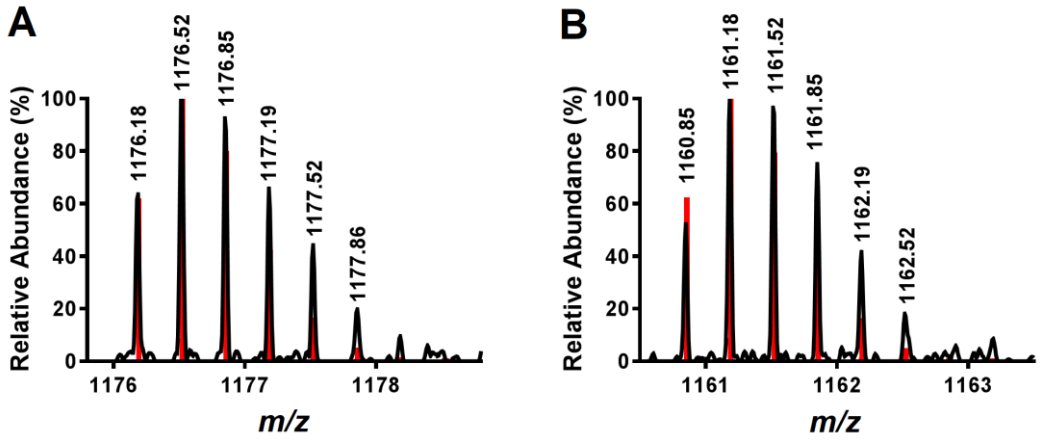

Figure S4. High-Resolution MS analysis of M1W V29A MftA modification. (A) M1W V29A MftA starting material, (B) M1W V29A Product 2.

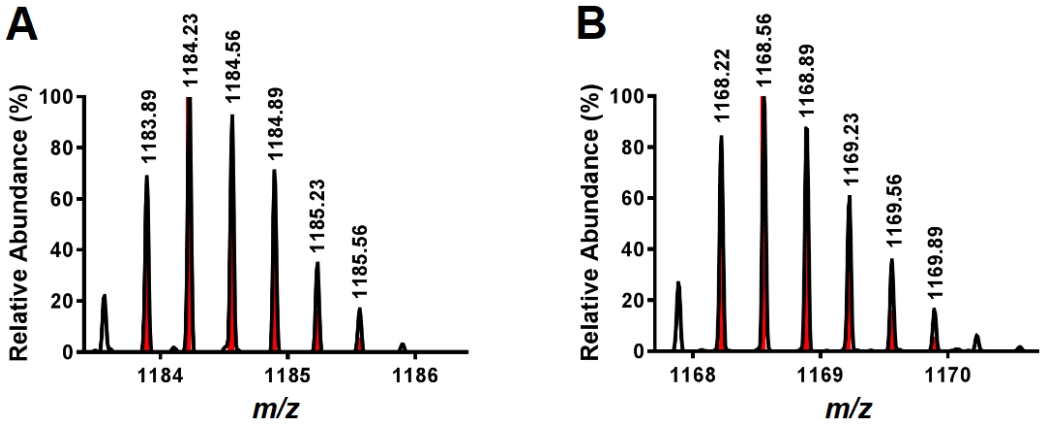

Figure S5. High-Resolution MS analysis of D_8-Val29 MftA modification. (A) D_8-Val29 MftA starting material, (B) D_8-Val29 Product 1.

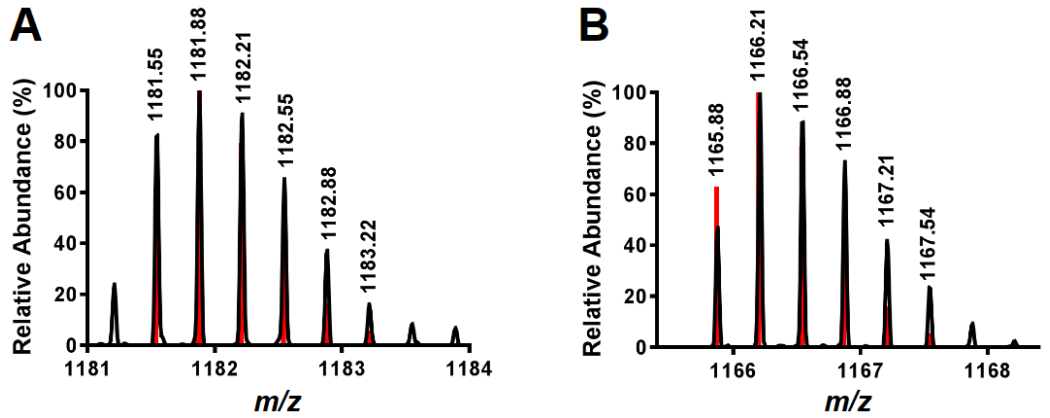

Figure S6. High-Resolution MS analysis of 3-D-Val29 MftA modification. (A) 3-D-Val29 MftA starting material, (B) 3-D-Val29 Product 1.

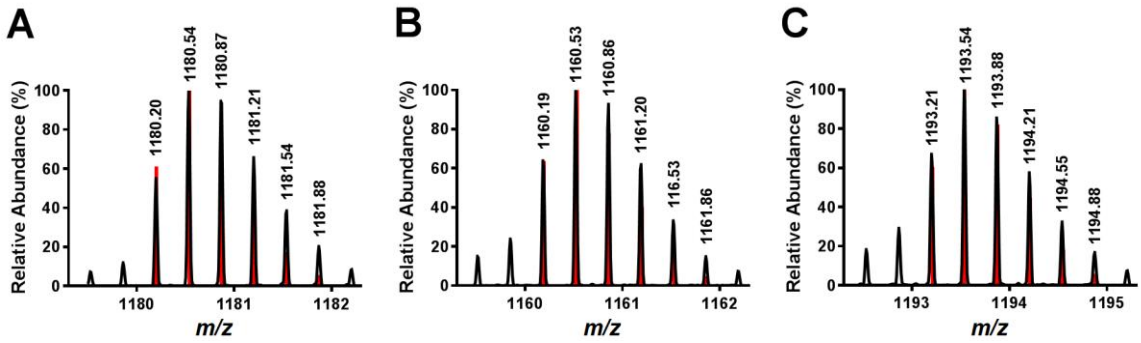

Figure S7. High-Resolution MS analysis of MftA C-terminal mutant starting materials. (A) M1W Y30F, (B) M1W Y30S, (C) M1W Y30W.